WATERSHED SEGMENTATION AND REGION

MERGING WITH APPLICATION TO

REMOTE SENSING

By

TAKASHI KOSHIMIZU

Bachelor of Science
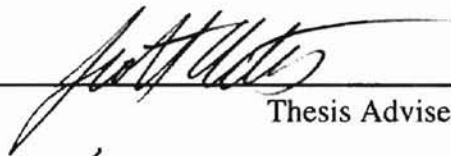
Tamagawa University

Tokyo, Japan

1990

Submitted to the Faculty of the
Graduate College of the
Oklahoma State University
in partial fulfillment of
the requirements for
the Degree of
MASTER OF SCIENCE
December, 1998

WATERSHED SEGMENTATION AND REGION

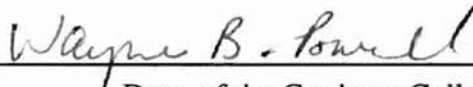# MERGING WITH APPLICATION TO

REMOTE SENSING

Thesis Approved:

_____
Thesis Adviser

_____

_____

_____
Dean of the Graduate College

ACKNOWLEDGEMENTS

Many people have contributed to this thesis, and I would like to specifically recognize several individuals. Dr. Scott T. Acton, my major professor, has supported me throughout entire this project. Through his contribution have been many, I want to thank him for his advice, constructive criticism, and gentle guidance. Additionally, I want to extend him my appreciation for allowing me, at times, self-reliant. I learned many things during this thesis, about academia, and about myself, and I attribute the positive result of this learning experience to him.

Other individuals within Oklahoma State university have also affected this thesis. I wish to acknowledge Dr. James West for his constructive advice and honesty. I want to thank Dr. Keith Teague for his friendship and encouragement, both in and out of the classroom. I want to express my appreciation to everyone associated with the Oklahoma Imaging Laboratory, and I with to specifically thank Mr. Andrew Segall, Mr. Joseph Bosworth, Mr. Anthony Hackner and Miss. Zhongxiu Hu for their many creative discussion. I have enjoyed interacting with these laboratory members and I also have been encouraged many times by these wonderful individuals.

Completion of this thesis has required personal sacrifices, and I want to acknowledge all of my friends and relatives for their understanding. Thanks to my

parents, Mr. and Mrs. Koshimizu, for their never-ending love and understanding. I want to thank Jones' family, especially Paul and Annette Jones. Their friendship, support and understanding have never come to end during my school work at Oklahoma State University.

TABLE OF CONTENTS

LIST OF TABLES

LIST OF FIGURES

Chapter1. Introduction

1.1 Overview

This paper studies an image segmentation technique, which considers the application and classification of satellite-sensed soil moisture images. Image segmentation is one of the essential and fundamental parts of image processing. The world of image segmentation is vast and there are various techniques.

As a first step, we start by reviewing the philosophical concept and the definitions, then clarify them to find a suitable technique for soil moisture image segmentation. The *watershed segmentation* is a powerful image segmentation technique. It is advantageous because it always forms closed and thin boundaries. Therefore, it is the main focus of this thesis. This image segmentation scheme is widely used by various types of images, such as medical imaging, texture segmentation, and object extraction. In this thesis, we apply this segmentation technique in order to classify the satellite-sensed ground soil moisture images. The original images have complex patterns, therefore our objective is to simplify the soil moisture image as much as preserving the original (soil moisture) distribution, *i.e.*, minimizing clustering error. However, in the practical application, there are two disadvantages associate with this algorithm - over segmentation and large computational costs. Our first goal in this thesis is to find a possible solution to these problems.

The region merging is a practical remedy for the over-segmentation, and a major focus of this thesis. Traditionally, region merging techniques are selected for specific applications and it was implemented in a heuristic manner. Therefore, we attempted to

1

establish a well motivated region merging technique for the watershed segmentation – this is the second goal in this thesis.

The demand for the application of image processing on satellite sensed imagery is growing, not only for the scientific research purposes, but also because it is widely utilized in our daily lives. Our study is initiated from the Earth Observing System, a project of NASA, which remotely monitors earth and studies its condition form a global point of view. One of the key topics in this research is the observation of the status and the transition of ground soil moisture from a global scale. The collected soil moisture data was processed to study global energy budgets and the water cycles of the globe.

Well organized ground soil moisture estimation techniques have been developed and applied recently. The soil moisture estimation techniques from the remotely sensed imagery are essential in mapping the status of the ground soil moisture over the global area. In this study, we chose an applicable technique and simplified it to draw soil moisture images from our satellite sensing data. The principle and process are fully explained in Chapter-3.

Unfortunately, the derived soil moisture images are less contrasted and quite uniform in grayscale distribution. Image segmentation of these images is not a simple task. When using conventional image segmentation techniques, it is difficult to yield meaningful segmentation results, due to the complexity of the image. The selection of a poor technique could cause an inadequate classification of soil moisture distribution. Therefore, the soil moisture segmentation technique has to be chosen with considerations.

In order to present a possible solution to these problems, a new and sophisticated region growing technique - the variational technique is introduced. The proposed

technique can be a possible solution to the issues of conventional region merging. Using the variational technique, an equation (energy function) is applied and the region merging progresses according to the energy function. Additionally, using the energy function, we have the ability to control the region scalability using a region scaling parameter. Being able to control the region scalability is essential in the image segmentation of this research. These details are fully explained in Chapter-4.

Once images are segmented, it is important to evaluate and measure the segmentation quality. If the segmentation results do not represent the original soil moisture distribution, the segmentation technique is useless. The formulation of the energy function contributes to the measurement and evaluation of the segmentation results. The development of a well motivated image evaluation technique is another important topic and it is our the third goal in this thesis. The segmentation results from the new approach are evaluated and compared to the conventional approaches according to the energy level. All of the results are shown in Chapter-5.

The importance of the image processing is growing with the development of digital computers and information technologies. Various image processing technologies are applied and utilized in our daily life, such as medical imaging, mass-production in industry, and the internet. This study focuses on just one section of the world of the image processing. But, proposing a possible solution to the existing issues, we would like to contribute a progress of the image processing. In the following chapter, Chapter-2, we start to review conventional image segmentation techniques and attempt to clarify the issues. The chapter also supplies the background of the watershed segmentation technique and the new image segmentation technique.

Chapter 2. Review of Literature

2.1 Introduction

This chapter provides the background for reviewing mainly three topics, which are the watershed segmentation(WS), morphological pyramid and region merging techniques. The first part of this chapter discusses philosophical definitions of image segmentation. The definitions will be a foundation for evaluating the image segmentation results. Choosing an adequate segmentation technique is an important starting point to yield meaningful results. In section 2.2, various image segmentation techniques are reviewed and examined for the applicability.

Another goal of this thesis is to establish a reasonable segmentation technique for the satellite sensed soil moisture (SM) images. The watershed image segmentation technique is mainly applied in this thesis. Therefore, the basic idea, the strengths, and the weak points are reviewed. In section 2.4., we will explain the concept of the image pyramid and the morphological pyramid which contribute the reduction of the computational costs. Development of a well established region merging technique is essential for the WS segmentation of the soil moisture images. In section 2.5, various region merging techniques are reviewed concerning the application of the SM images.

Lastly, section 2.6 reviews the ground soil moisture estimation techniques from remotely sensed imagery. Several possible soil moisture estimation techniques are reviewed and the characteristics are clarified. In the following section, we explain the basic concept of the image segmentation criteria.

2.2   Review of Image Segmentation Techniques

2.2.1   Image Segmentation Criteria

As the first step in finding a suitable segmentation technique for the soil moisture images, we summarize and clarify the philosophical definition of image segmentation. Without understanding the fundamental concept of image segmentation, it would be difficult to evaluate the segmentation results.

There are several viable definitions of image segmentation. Gonzalez (Gonzalez, 1992) defined image segmentation as "subdividing an image into consistent parts or objects". Castleman mentioned an alternative definition as "decompose an image into meaningful parts with respect to a particular application" (Castleman, 1996).

If the target object is clearly known, the objective of segmentation is to segment the target features from the background. Unfortunately, the target objects are not always clearly identified (our soil moisture images, for example). In order to illustrate the characteristic of our SM images, we compared two images. In Fig.2.1(a), the target object (a swan) is clearly identified. The objective of segmentation of this image will be segmenting the swan. In contrast to the swan image, a soil moisture image is shown in Fig.2.1(b), neither a clear target nor a crisp boundary are observed. Thus, for the segmentation of the soil moisture image, we have to prepare an adequate image segmentation technique. Because of the absence of the target image, the segmented results have to be measured at an appropriate scale. If the swan is segmented, even visually it is possible to evaluate the segmentation results. But, how should we evaluate the segmentation results of the soil moisture image? It is much difficult to define *meaningful* or *sound* segmentation results of the soil moisture image, because of the

5

absence of a clear target. This is the reason we want to established a segmentation quality evaluation technique in this research.

Fig.2.1 An comparison of well target identified image and target absence image.
Fig 2.1(a) has a clear target object a swan,
Fig 2.1(b) does not have a *clear* object in the image.
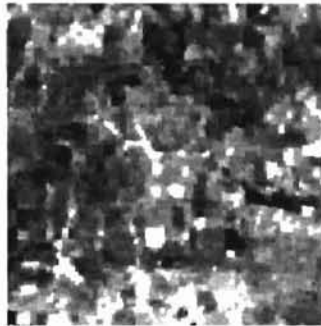
Fig2.1(a) A Swan Image   Fig.2.1(b) A Soil Moisture Image

Before exploring the topic, let us list the properties of a *good* segmentation. The properties below have been used as a guideline to evaluate the segmentation results. According to Haralick (Haralick, 1992), general segmentation procedures tend to obey the following properties:

1. Segmented regions of an image should be uniform and homogeneous with respect to some characteristic, such as gray level or texture condition.

2. Region interiors should be smooth and without holes or spots.

3. Adjacent regions should have significantly different values with respect to the characteristic on which they are uniform.

4. Boundaries of each segment should be simple, closed, and spatially accurate.

Haralick also mentions that it is difficult to achieve all the desired criteria. Therefore, we need to carefully choose the segmentation technique that is especially suitable for our soil moisture image segmentation. In the following subsection, we review several segmentation techniques and evaluate their suitability for the soil moisture image segmentation.

6

2.2.2 Image Segmentation Techniques

In general, image segmentation algorithms can be categorized by two different approaches: *edge-boundary* approach and *region-based* approach. In the edge-boundary approach, one seeks to identify edge pixels and link them together to form the image boundaries. The edge-boundary approach seeks discontinuity over the image. It directly seeks edges or boundaries in the image and eventually divides the image based on the boundaries.

Fig.2.2 Two Image Segmentation Approaches

Region-Based Approach	Edge & Boundary Approach
SEEK SIMILARITY	**SEEK DISCONTINUITY**
• Global thresholding	• Robert edge detector
• Adaptive thresholding	• Prewitt edge detector
• Split and Merge	• Sobel edge detector
• Watershed	• Laplacian

Image Segmentation
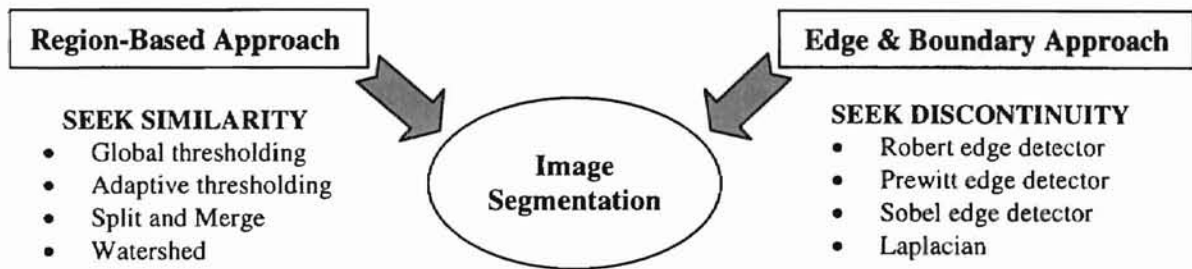
The second category, the region-based approach seeks region or pixel similarities. Using a threshold or other statistical values, it segments an image into homogeneous regions. There are various image segmentation techniques among this category. In the following subsection, we will examine the strengths and the weaknesses of each image segmentation technique to clarify if they are applicable to our particular needs.

2.2.3 The Edge and Boundary Approach

An edge is the boundary between two regions where has significant graylevel differences occur. This approach seeks the edges by directly examining each image pixel and its immediate neighbors to determine whether the pixel can be an edge. Pixels

exhibiting the required characteristics are labeled *edge points* and the image that indicates

the presence of edges is called the *edge map* or the *edge image*.

The basic idea behind the edge-detection technique is the computations of the

local derivative operation. This concept is shown in Fig.2.3 with a simple example.

Fig.2.3 An illustration of the basic edge detection mechanism

(a) Original Images   (b)The Magnitude   (c) The First derivative   (d) The Second derivative
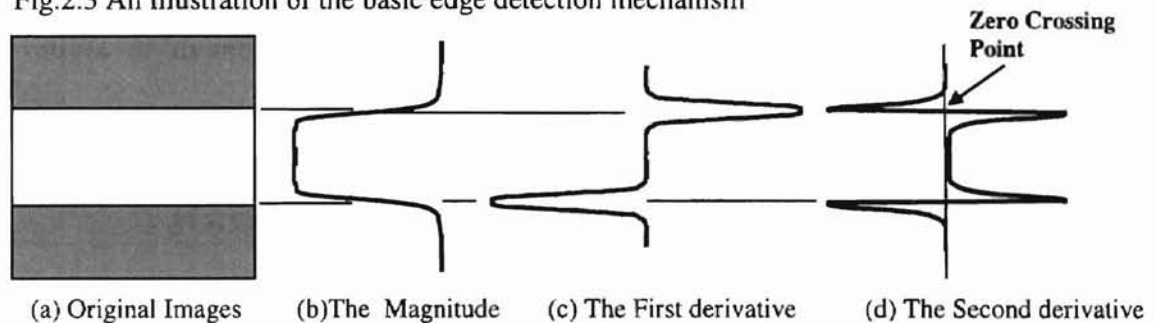
Fig.2.3(a) is a simple gray-level image, where the dark area is gradually changing to the

bright area and the magnitude intensity is shown in Fig.2.3(b). The first derivative of the

magnitude can be drawn as in Fig.2.3(c). The peaks locate the middle of the gray-level

transition, and is the location of the edges. In the first derivative, Fig2.3(c) the peak

locates the middle of the transition, so it is difficult to detect the exact peak locations

when the image has complex features. This can be simplified by taking the second

derivative of the magnitude, Fig.2.3(d) and locating the zero-crossing points. The first

derivative is obtained by using the magnitude of the image gradient and the second

derivative is similarly obtained using the Laplacian operator as shown in the following

subsection.

Gradient Operators

Given an image **I**, with $I(x, y)$ is the intensity at (x, y) in the image **I**. The gradient

magnitude of an image $I(x, y)$ can be shown as

$$\nabla I = [D_x, D_y]^T = [\frac{\partial I}{\partial x}, \frac{\partial I}{\partial y}]^T.$$

The gradient magnitude is given by

$$\nabla I = mag(\nabla I) = [D_x^2 + D_y^2]^{1/2}.$$

From the above equations, the gradient magnitude is obtained from partial derivatives $\partial I/dx$ and $\partial I/dy$. If we take the derivative of two spatial neighbors we can make a Robert edge operator, such as

$$g(x,y) = \{[\sqrt{I(x,\ y) - I(x+1,\ y+1)}]^2 + [\sqrt{I(x+1,y) - I(x,y+1)}]^2\}^{1/2},$$

$$= mag(\nabla I) = [(\frac{\partial I}{\partial y})^2 + (\frac{\partial I}{\partial y})^2]^{1/2},$$

where $I(x, y)$ is the input image with a location of (x, y). This is simply operating a cross differentiation on two adjacent points. In the practical application of the image processing, these equations are translated into the kernels or operators. These operators are convoluted with the original image to detect image edges. Sobel and Prewitt edge detection operators are one of the practical examples. Shown below is an example of a formula to show how the Prewitt operator works with a 3x3 kernel.

$$g \approx |(z_7 + z_8 + z_9) - (z_1 + z_2 + z_3)| + |(z_3 + z_6 + z_9) - (z_1 + z_4 + z_7)|,$$

$$= |D_x| + |D_y|,$$

$$D_x = (z_7 + z_8 + z_9) - (z_1 + z_2 + z_3) \text{ and } D_y = (z_3 + z_6 + z_9) - (z_1 + z_4 + z_7).$$

This operation can be implemented by convoluting the following *mask* with the original image.

The 3x3 mask is called the *Prewitt-operator* as shown in Fig.2.4.

Fig.2.4 The Prewitt-operator
kernels. (a) is the layout of the
kernel. (b) and (c) indicates
example of the kernel.

Z_1	Z_2	Z_3
Z_4	Z_5	Z_6
Z_7	Z_8	Z_9

(a)

-1	-1	-1
0	0	0
1	1	1

(b) : D_x

1	0	-1
1	0	-1
1	0	-1

(c) : D_y

The Sobel operator uses the same 3x3 area as Prewitt, but with a slight change in the coefficients. Each mask is shown in Fig.2.5 with the center pixels of the Sobel operator assigned more weight. The original formula and the convolution kernel are shown as follows.

$$D_x = (z_7 + 2z_8 + z_9) - (z_1 + 2z_2 + z_3) \text{ and } D_y = (z_3 + 2z_6 + z_9) - (z_1 + 2z_4 + z_7).$$

Fig.2.5 The Sobel
operator kernels

-1	-2	-1
0	0	0
1	2	1

D_x

1	0	-1
2	0	-2
1	0	-1

D_y

The Laplacian Operator

The *boundary approach* attempts to find the edges directly by seeking high gradient magnitudes in the image. As in the previous example, the boundaries are detected by running a boundary detection window (kernel) over the gradient magnitude image. Laplacian edge detection is one of the example and it is a scalar second-derivative operator. In two dimensions, it is defined as

$$\nabla^2 I(x, y) = \frac{\partial^2}{\partial x^2} I(x, y) + \frac{\partial^2}{\partial y^2} I(x, y).$$

This operation is commonly implemented by a convolution kernel. Since it is a second derivative operator, the edges are located on the zero-crossing point. The locations of the zero-crossing points are supposed to correspond to the edge locations in the original

10

image, in Fig.2.3(d). This operation is noise sensitive, thus when noise exists in the image, an additional noise elimination function is usually applied. (Castleman, 1996).

One of the advantages of the edge-boundary approach is the simplicity and the low computational costs. Yet, this technique has serious disadvantages - these operations seldom form closed connected boundaries. Eventually, these edge detection approaches require additional edge-linking steps to form closed contours of the objects. Edge-point linking is the process of finding missing edges to form close contours. This process is very tedious and has the potential to create false edges. Thus, these edge and boundary detection approaches would not be appropriate in our study, especially for the soil moisture image segmentation.

Fig.2.6 is the image segmentation results on an Aluminum-grain image by the Sobel edge detector. In this experiment we used two levels of threshold value, $T = 0.01$ and 0.02. The segmentation results are shown in Fig.2.6(b) and 2.6(c) respectively. These segmentation results (edge map) show unclosed contours. When the threshold value is increased, trivial edges emerge, in Fig.2.6(c), yet still the contours are not closed. So, just increasing the threshold value can not be the solution of the edge linking problem.

Fig.2.6 Segmentation results by the Sobel edge detection operator

(a) Original Image   (b) The edge map at T=0.01   (c) The edge map at T=0.02
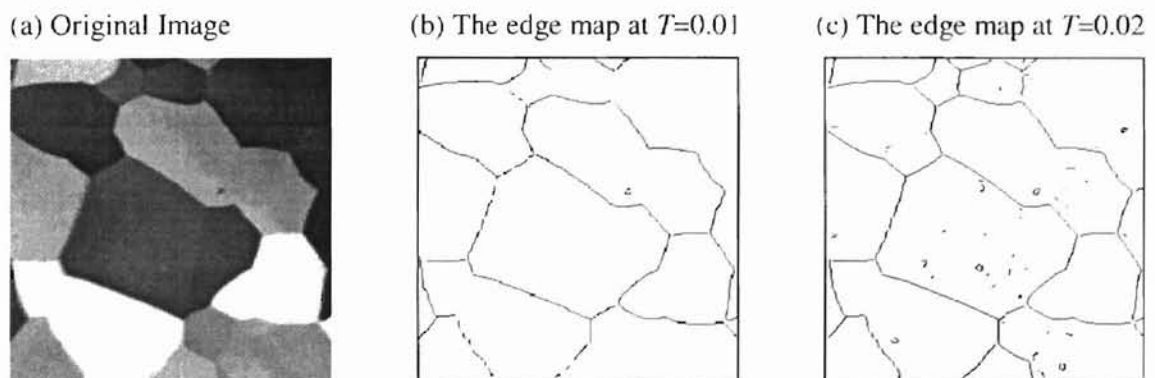
2.2.4 Region-based Approach

The previous edge-boundary approach sought discontinuity of the image pixels and detected the edges and/or boundaries to segment the image. In contrast, the region-based approach seeks *similarity* of each of the image elements or regions. In this subsection, three possible applications are introduced and examined - thresholding, spirit and merge, and watershed segmentation.

Thresholding

Thresholding is a useful segmentation technique if the image has solid objects and contrasting background. This approach is simple, requires little computation and sometimes makes closed regions with connected boundaries. Thresholding works well if the objects of interest have uniform gray levels and the rest of the background has a different but uniform graylevel. When one threshold value is used to segment an entire image, it is called a global threshold. Sometimes a single threshold value is not appropriate to segment a complex image. In the adaptive thresholding, first the entire image is divided into several sub-regions, and each threshold value is selected depend on the sub-regions. In both cases, the selection of the threshold values depend on the shape of the histogram. When the histogram is bimodal, usually the threshold value is chosen at the bottom of the valley (Castleman, 1996).

Unfortunately, the thresholding approach has to dependent upon the shape of the histogram. Fig.2.7 shows the

Fig.2.7 The histogram of a SM image

12
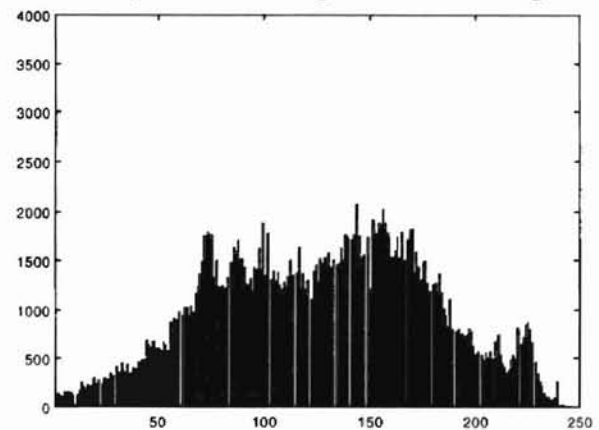
histogram of the soil moisture image in Fig.2.1(b). The shape of the histogram is more complex than a bimodal distribution. So, the first issue in this approach is the selection of the threshold value.

Next, if we arbitrarily select multiple thresholds in even intervals, how would the image be segmented? Let us assume we evenly subdivide (slice) this histogram into 10 sub-parts to segment the image into 10 gray-scale classes. But how will the segmentation result look? The worst aspect of this approach is the ignorance of size and spatial location of the regions. The histogram approach does not consider the spatial location of the clusters (regions). Consequently, the segmentation scheme forms small scale and/or large scale regions by chance, and we are not able to control the regions scalability (size of the regions) at all. The major disadvantage of the thresholding approach is the absence of region scale controllability.

Split and merge

This algorithm creates regions by splitting and/or merging the regions using a similarity criterion that is sometimes called a predicate. Initially an original image is subdivided into arbitrary, disjointed sub-regions and then merge and/or split the regions to satisfy a given predicate, P. The original image is successively subdivided into smaller and smaller quadrant regions until each region meets the predicate. Using the same manner, regions can be merged if the merged region can meet the predicate. Therefore, this scheme continues merging or splitting regions until each region meets a given similarity criterion. What is the disadvantage in this scheme and how do the segmentation results look? First of all, the selection of the predicate is done in a heuristic manner, and practically it is difficult to select a meaningful value. Second, this scheme also does not

consider the region scalability (region size). This algorithm isolates extremely high and low grayscale small regions in the result image. Noise in an image tends to have the same characteristics (small but extremely high or low intensity). Therefore, this scheme is insensitive to the noise and does not effect them! The lack of control over the region scalability is a pitfall of this algorithm as well. Hence, we need to find a more intelligent image segmentation approach.

In the following part we will explain the watershed segmentation algorithm. Our soil moisture segmentation technique is based on the application of the WS algorithm. First, we will summarize the characteristics, the strengths and the weaknesses. Then we propose possible solutions for the weak points.

Advantages and Pitfalls of the Watershed Segmentation

The Watershed segmentation is one of the region-based image segmentation algorithms which subdivides an entire image into small homogeneous regions. This algorithm was originally developed end of the 1980's, then Meyer(Meyer and Beucher, 1992), Vincent(Vincent and Sollie, 1991) and Gauch(Gauch and Pizer, 1992) has modified the algorithm to more practical use. The watershed algorithm has two main advantages compared to other segmentation techniques. First, it automatically produces thin and closed boundaries. Thus, this algorithm never requires additional time consuming contour-tracking or edge-closing processing. That is a strong incentive when choosing an image segmentation algorithm. As a second advantage, the watershed algorithm automatically subdivides an image into small and highly homogeneous regions, which is called a watershed mosaic image. Additionally, the boundaries are zero thickness, because the watershed segmentation defines the boundaries as region

14

differences. This is a large advantage of the region based approach. These two properties are strong motivators as to why we assign this algorithm for the soil moisture image segmentation. In order to compare the segmentation results, Fig.2.8 demonstrates a segmentation for the same Aluminum-grain image as in Fig.2.6.

As the boundary image shows in Fig.2.8(c), the contours are all closed and no trivial edges exist. Compared to Fig.2.6(c) the difference is significant. Nevertheless, the watershed algorithm is not impeccable - it has a couple of disadvantages. The watershed segmentation algorithm is highly sensitive to local graylevel variations, thus usually resulting in a highly over-segmented image. Fig.2.8(c) was originally over-segmented, and this result was given after a region merging process, which will be explained in Chapter-4. Another drawback of direct application of the watershed segmentation is the large computational cost.

Fig.2.8 Segmentation results from the Watershed segmentation

(a) Original Image   (b) The Mosaic Image   (c) The Boundary Image
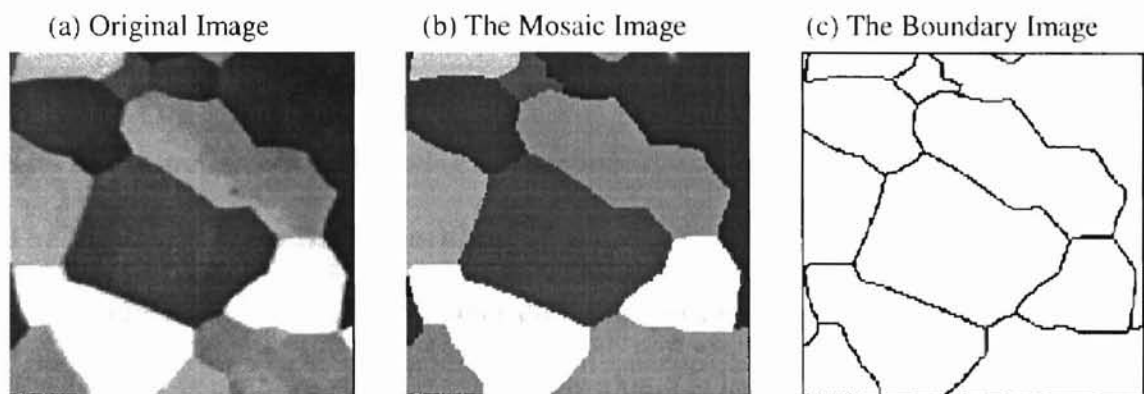
Historically, various techniques have been studied in order to overcome these drawbacks, but the best solution has not yet been found. We were challenged in this thesis to find the best solution for the two issues. These techniques are discussed with a demonstration in Chapter-4. In the following table, the strengths, the weaknesses and our solutions for the watershed segmentation algorithm are summarized.

Up to now, we reviewed several image segmentation techniques clarifying the strengths and weaknesses. The following sub-section briefly reviews the idea of the WS segmentation algorithm.

Table 2.1 : WS segmentation - the strengths, weaknesses and possible solutions

Strengths	Weaknesses	The solutions
• Closed contours and regions • Thin boundaries • Draw mosaic image • Applicable to complex images	Over-segmentation High computational cost	Region Merging Image Pyramid

2.3 The Watershed Segmentation

The concept of watershed is drawn from topographical analogy. Consider the gray level intensity of an image as a topographic three-dimensional relief. Assuming we drop rain over the geographical area, water would drain from higher points to lower points as we see in nature. Then we cluster all points that drained to the same local minima. By the clustering process, we can draw watershed regions and their boundaries. This process is called the minimum following algorithm. The brief concept of this algorithm is explained with an illustration in the following sub-section.

The Minimum Following Algorithm

The minimum following algorithm, introduced by Gauch and Pizer (Gauch and Pizer, 1993), is one type of a watershed algorithm. Let us assume a gradient magnitude of an image is a geographical surface. The first process in this algorithm is finding the local minima. The local minima can be detected at the lowest points among the 3x3 spatial neighbors, and they are assigned unique identity numbers. Then, we attempt to drop water over the gradient magnitude image relief to detect where the rain drops are drained. The rain drop will seek lower altitude and eventually meet a local minimum. Once the

16

The rain drop will seek lower altitude and eventually meet a local minimum. Once the rain drains to a local minimum, the unique identity number is returned to the original starting point. These points are called catchment basins. This process is applied to all of the points over the image relief. Once all catchment basins have been labeled, watershed boundaries are drawn by simply detecting the difference of the catchment basins. In other words, watershed boundaries are borders of the catchment basins. Fig.2.9 illustrates a local minimum, catchment basin, and the watershed boundaries in a simple image relief. As we showed segmentation results in Aluminum-grain segmentation in Fig.2.8, the watershed boundaries can be easily drawn by detecting the differences of the catchment basin number.

Fig.2.9 An illustration of WS

Watershed lines

Catchment basin

A Local minimum

Historically, there is another variation of watershed, which is called the immersion algorithm. According to the immersion algorithm, the whole gradient magnitude image relief is immersed into a large water tub and then the flooding patterns are recorded to draw the pattern of the segmentation. This algorithm was introduced by Vincent (Vincent and Sollie, 1991) and sometimes applied by other researches such as Meyer and Beucher (Meyer and Beucher, 1992). But, the applied images in the research were simple compared to our SM images. Additionally, this approach requires complex false edge elimination processing. Dobrin (Dobrin *et al.*, 1994) studied the immersion algorithm and reported the possibility of the false boundary occurring by the algorithm. The minimum following algorithm overcomes the weak point

(the creation of false boundaries) of the immersion method. Also, the minimum following algorithm is simpler to implement. Since the creation of false boundaries is a serious segmentation issue, we have focused on the minimum following algorithm in this study.

In this subsection we reviewed the mechanism and key characteristics of the watershed segmentation. In the following section, we will review possible remedies for the two issues that are mentioned earlier – large computational costs and over-segmentation. The application of the image pyramid is one possible solution for the reduction of the computational costs. In the following section, the basic concept of the image pyramid is explained with an illustration.

2.4   The Morphological Pyramid

Image pyramid is a scale space technique. Sometimes original images contain extra information, such as insignificant edges or noise. This morphological filtering and sub-sampling process leaves only significant information and eliminates noise and trivial information of the image.

A morphological pyramid is constructed by successive filtering of the original image with morphological operators. By repeating this step, the original image size will be reduced by sub-sampling factors. For example, two-to-one pixel sampling along each dimension makes a quarter of the original image size.

Fig.2.10 Morphological Image Pyramid

Sampling

Sampling

128x128

256x25

Size = 512x512

18
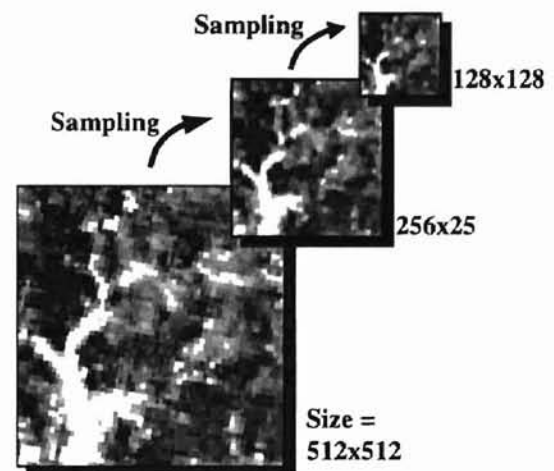
Recurrence of this process creates a multi-resolution image pyramid, shown in Fig.2.10. When a morphological filter is used during the sampling process, the image pyramid is often called a morphological multi-resolution pyramid (Hejimans and Toet, 1991).

The reduction of the computational cost is the major incentive for the application of the image pyramid. Processing a small image takes less computational time. Remember that over segmentation is another pitfall of watershed segmentation. Region scalability is also observed from the multi-resolution approach, because it creates a scale space. Thus, using the morphological pyramid, both disadvantages could be minimized. In the following subsection, further characteristics of morphological pyramid are reviewed, such as, the filter type, the filter size and the sampling conditions.

Implementation of the Morphological Pyramid

The selection of the morphological filter is important. The size and filter type directly affect the sampled image. The objective of the morphological filtering is that it removes trivial edges while eliminating the noise. If the size of filter kernel (structure element) is too large, it could destroy important contours. Morales and Acharya (Morales and Acharya, 1995, 1991) intensively studied the relationship of morphological sampling filter and its effects. According to the study, the sequential open-close filter with the smaller structure element is the best choice to preserve the edges. From the study, it has been shown that sequential open-close filtering has less distortion and smoothes the image better than direct application of a large structural element. The same sequential open-close filtering technique has been applied in our multi-resolution morphological pyramid.

19

In the below, the concept of open-close morphological filtering is reviewed. Two fundamental operators, erosion and dilation make up all morphological filters. When the original image is given by $\mathbf{I}$ and a structural element $\mathbf{K}$, dilating an image $\mathbf{I}$ with the structuring element $\mathbf{K}$ is defined by

$$(\mathbf{I} \oplus \mathbf{K})(x) = \max\{I(y) \mid y \in \mathbf{K}\}.$$

Dilation performs a moving local-maximum operator, while erosion is a moving local-minimum operator, thus the erosion is defined by

$$(\mathbf{I} \ominus \mathbf{K})(x) = \min\{I(y) \mid y \in \mathbf{K}\}.$$

By using these fundamental operators, two higher order operators are established. The opening of an image $\mathbf{I}$ by structuring element $\mathbf{K}$ is defined as

$$\mathbf{I} \circ \mathbf{K} = (\mathbf{I} \ominus \mathbf{K}) \oplus \mathbf{K} \quad, i.e., \text{ dilation then erosion by } \mathbf{K},$$

and the closing of image $\mathbf{I}$ by structuring element $\mathbf{K}$ is defined as

$$\mathbf{I} \bullet \mathbf{K} = (\mathbf{I} \oplus \mathbf{K}) \ominus \mathbf{K} \quad, i.e., \text{ erosion then dilation by } \mathbf{K}.$$

An open-close filter is made by cascading open and close operators $i.e.$,

$$\text{Open-Close Operation} \equiv (\mathbf{I} \bullet \mathbf{K}) \circ \mathbf{K}.$$

When a morphological pyramid is constructed with an open-close filter, we can denote the image pyramid level I_L by

$$I_L = [(\mathbf{I}_{(L-1)} \bullet \mathbf{K}) \circ \mathbf{K}]_{\downarrow S},$$

where L is a pyramid level, $\mathbf{K}$ is a structuring element. For example, $[\cdot]_{\downarrow 2}$ represents a sub-sampling by a factor of two. If we apply $S = 2$ then the size of the upper layer pyramid image is one-half of the sampled image in each dimension. Furthermore, the

higher the image layer, the more significant the edges that remain, because of the iterated open-close filtering (Heijmans *et al.*, 1991).

This subsection has explained the mechanism and objective of the image pyramid. When the idea of the image pyramid is applied to the watershed segmentation, it is called the multi-resolution watershed segmentation approach. The multi-resolution approach contributes to reduce the computational time and to control the region scalability. Our application and the detail of the multi-resolution watershed pyramid will be explained in Chapter-4.

In the following section, we reviewed several regions merging techniques. By reviewing these techniques we clarify the weaknesses and the strengths of each region merging technique for the applicability to soil moisture segmentation.

2.5 Region Merging Techniques

A region merging process is an essential part in the practical watershed image segmentation process. There are two goals in the region merging. The first goal is to find an adequate region merging technique for the soil moisture imagery. The second goal is to establish a suitable quality measurement scale for the segmented results.

Historically, several region growing and merging techniques have been used to overcome the over-segmentation and to yield a reasonably segmented image. Unfortunately, these techniques have been applied in a heuristic manner and for individual applications. Therefore, we attempt to establish a well motivated region merging technique. The following subsection reviews several region merging techniques.

These techniques are the single linkage region growing scheme, edge-strength seeking, the marker-based segmentation scheme, and the variational method.

The Single Linkage Region Merging Technique

The single-linkage region merging scheme assumes each region or image pixel is a node of a graph. Given a similarity criterion, regions are formed by clustering as all of the connected pixel sets meet the criterion. Sometimes, the similarity is measured by using region graylevel or other statistical numbers, such as standard deviation or likelihood ratio(Haralick, 1992).

Fig.2.11 An illustration of the Single Linkage Region Growing Algorithm. Fig 2.11(a) illustrates original pattern with a clustered region. Fig 2.11(b) indicates merged region with new assigned region value.

Fig.2.11 (a)

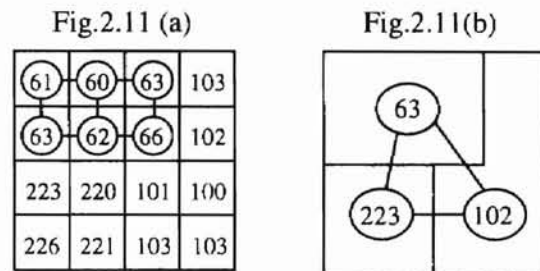|			
61	60	63	103
63	62	66	102
223	220	101	100
226	221	103	103

Fig.2.11(b)

Fig.2.11(a) demonstrates this idea with a simple illustration. In the figure, the gray value of each pixel is shown and the six pixels are already grouped, where each node is connected by a line. In this example, pixels are connected by lines if their values differ by less than 10.

One advantage of the single-linkage region clustering scheme is the simplicity, which means the region comparison needs only the neighborhood regions. Historically, sometimes this concept has been used in the watershed region merging process. Vincent also expanded the idea and applied this scheme to suppress over-segmentation with recursive merging. The recursive merging varies the threshold (merging criterion) values, which start from low, then gradually increased to merge additional regions. The recursive merging can control the merging order according to the region similarity. Because the

threshold value is gradually increased, highly similar regions are merged in the early stage, and dissimilar regions are merged later. The order is sometimes called the merging hierarchy.

Once regions are merged, the region graylevel and the graphs are updated to the newly emerged regions, as depicted earlier in Fig.2.11(b). The termination of merging occurs when a desired number of regions or objects are obtained. This conventional merging technique is applied to segment our SM images. The details of the experimental results are explained in Chapter-5.

Edge Strength Seeking

This approach focuses on adjacent edge magnitudes instead of the region graylevel value. When an edge magnitude value is less than a given edge threshold (criterion), the connected regions are merged. These edge strengths are detected by applying an edge detection operator over the segmented image. Beucher and Meyer extended this idea with a clustering hierarchy. The clustering starts by merging the lowest edges. Once all the weak edges are merged, the threshold is gradually increased and the recursive merging process continues. Thus, the clustering process produces a hierarchy of region merging (Meyer and Beucher, 1990).

A drawback of this approach is that it has to depend on the edge detection process. If the image is noisy, this technique has a chance to produce false edges. As we reviewed in section 2.3, the edge detection process is very sensitive and rarely forms closed contours. For these reasons, we will not apply this approach for our region merging scheme.

Marker-Based Segmentation

The marker-based segmentation is sometimes used to suppress watershed over-segmentation. The marker has two types, an inner marker and an outer marker. The inner marker is located inside the target object and is used to group the region inside the target object. The outer marker is located in the background and is used to group the background regions (Dobrin, Viero *et al.*, 1994). The marker based clustering is applicable only if the image is simple in its construction and contains a target object and background. Unfortunately, our soil moisture images have complicated features. Hence, the marker-based segmentation does not seem to be suitable for the segmentation of our soil moisture images.

The Variational Technique

The variational technique is quite different from previous region merging approaches. This method translates an image segmentation into an equation. The method formulates a mathematical equation and the image segmentation is progressed according to the equation (Morel and Solimini, 1994). Generally, the energy equation totally depends upon the user's interest, so the image energy should measure based on what the user wants to measure.

Therefore, the first task in this method is to formulate an appropriate energy equation that represents our region merging process. We focused on two terms, the region smoothness and the number of regions, because the two terms represent opposite status. Using these terms we attempted to formulate our energy equation. The detail is fully explained in Chapter-4. The formulation of the energy equation has another advantage; it enables us to measure the quality of the segmentation. The segmented images can be

evaluated according to the image energy. The new region merging technique is a well motivated scheme which contrasts most of the historical heuristic region growing approaches.

This subsection has reviewed and clarified the strengths and weaknesses of the region merging techniques. Most of the techniques compared the similarity of neighbor pixels, or regions, using graylevel similarity or statistical values. Unfortunately, our soil moisture images are complicated and the graylevel vary gradually. Thus, we need to develop a stronger merging algorithm than what exists now. Our new merging scheme, an application of a variational technique, is fully studied and compared in Chapter-4. From the conventional merging scheme, we applied the single region linkage with recursive merging techniques for the soil moisture image segmentation.

Up to now, we have reviewed image segmentation techniques and region merging schemes to find the best approach for the soil moisture images. Continuing in the next section, we will review the soil moisture estimation techniques.

2.6   Soil Moisture Estimation Techniques

This subsection reviews general concepts of Soil Moisture (SM) estimation techniques from remotely sensed imagery. Estimation of SM from satellite imagery has been an important research topic for related researchers. It has been studied extensively by agricultural, hydrologic, environmental and soil scientists. The estimation techniques from these studies tend to formulate complicated models. Various local weather conditions and hydrological parameters have to be considered, such as wind condition, soil textures, canopy coverage, humidity, amount of rain, and amount of solar radiation.

One of the issues of applying these comprehensive models is that it is difficult to obtain all of the parameters. Thus, we attempted to find relatively simple SM estimation models without losing significant SM information. Here, we review several SM estimation techniques and then we introduce the *Triangle method*.

Estimation SM using T_s and TM 5/ TM 7

The first approach of SM estimation was simply using the relationship between satellite measured surface radiant temperature (T_s) and the ground wetness. The Heat Capacity Mapping Mission (HCMM) satellite was launched in 1978, which was the first satellite to be devoted to acquiring high-resolution thermal data. From the data received, the relationship between the ground SM content and observed T_s (over the bare-soil) was studied. Because, the wet regions tend to have the lower temperature, this study measured the surface temperature from satellite to estimate the ground water content. The actual content of the ground soil water (ground truth data) was measured by the gravimetric manner (the ratio of the mass of water per the mass of the sampled dry soil). A handful of ground soil samples were collected over the satellite sensed region and the water contents were measured in the laboratory. This study shows the correlation of T_g (*calibrated ground temperature*) and the soil water contents was $r^2 = 0.74$ with a non-linear relationship (Heilman and Moore, 1982). The research also concluded that the measuring of SM was affected by local weather conditions and soil texture. The study has been done only over the bare soil, therefore the SM estimation over vegetated regions will need a more practical technique.

In the end of the 1980's, estimation of SM from the band-ratio approach was examined. The band-ratio analysis uses the combination of spectral bands rather than

26

single band data. Several researchers implied that the ground wetness could correlate to the TM5/TM7 ratio (TM stand for Thematic Mapper, spectral sensors on Landsat). Musick extended this idea and examined the TM5/TM7 and ground soil water contents under various soil types. From his study, the wetness ratio had weak linear relations to the water contents of sampled soil with correlation of $r^2 = 0.48$. The research also suggested that the TM5/TM7 ratio was largely affected by the soil texture and soil type (Musick and Pelletier, 1988). This is one of the disadvantages of the estimation scheme, because it is difficult to convert the soil texture type to parameters. Next, we focused on another estimation technique that is called the *Triangle method*, which was originally developed by Carlson (Carlson, 1991). This model estimates ground SM levels from the relationship between surface radiant temperatures(T_s) and the normalized difference vegetation index (NDVI). This model is simple, yet significant amounts of SM can be estimated.

Estimation of SM from T_s versus NDVI and The Triangle Method

In the early 1990's, it was realized that ground surface water content could be estimated from the relationship of T_s and NDVI. The relationship of NDVI versus T_s has been studied by several researchers and recently have shown that there is a high correlation between remotely sensed vegetation levels and surface temperature (Goward and Hope 1990; Carlson *et al.*, 1990; Price 1989). This approach uses two parameters – NDVI and TM band-6, to estimate ground soil moisture level. The NDVI measures the vegetation level of the ground, and the Landsat TM band-6 measures the surface radiant temperature T_s.

The triangle method is a technique that estimates SM levels from the distribution of the scatter plot. A scatter plot draws the relationship of NDVI versus T_s. Isopleths are defined as the lines that have the same SM level over the scatterplot. Therefore, if we draw the isopleths over the scatterplot, we can find SM level. From Carlson's research (Carlson *et al.*, 1990), the isopleths are drawn by SVAT (soil-vegetation-atmosphere transfer) model, which considers local weather and hydrologic parameters. But in our triangle method, we simplified the concept and attempted to draw linear isopleths over the scatter plot using a relatively small area. The details of the process will be explained with illustrations in the following chapter.

2.7 Summary

In this chapter, we attempted to seek appropriate image segmentation techniques for soil moisture images. Reviewing the possible image segmentation techniques, we found large advantages in the watershed segmentation technique – it forms closed and thin segmentation boundaries. Unfortunately, there are two weak points in the algorithm – large computational costs and over segmentation issues. For a possible remedy for the computational costs, we use the image pyramid approach. By using the scale space (the pyramid approach), significant computational cost can be reduced.

The region merging technique is a possible solution to the over-segmentation issue. Because the structure of the soil moisture image is complex, we attempted to develop a new region merging technique by applying the variational technique. This merging technique is advantageous compared to the conventional technique, because of the formulation of the equation. By forming the equation, the ability to control the region

scalability is obtained. The success of the variational technique largely depends on the formulation of the energy equation. In this research we focused on the region smoothness and the cardinality (the number of regions) of the image. The second advantage of the energy function is the ability to measure the segmentation quality. For SM image segmentation, the evaluation of the segmentation results are extremely important. Because poor image segmentation techniques could yield incorrect soil moisture distributions in the segmentation. The details of the process are fully explained in Chapter-4.

Various scientists have studied soil moisture estimation technique from satellite imageries. In this research, we selected Carlson's soil moisture estimation technique – the triangle method, because it enables the estimation of surface water contents with high reliability. For the practical application of the estimation model to our research, we simplified the model by using smaller regions. The details of the process are explained with illustrations in Chapter-3.

Chapter 3.

The Soil Moisture Estimation Technique from Satellite Imagery

3.1   Introduction

This chapter introduces and demonstrates the soil moisture estimation technique from satellite imagery. The nature of the original satellite imageries, the mechanism of the soil moisture estimation technique, and our simplified method are fully explained with examples.

The potential for soil moisture measurement via satellite was realized about two decades ago. Only recently, have the estimation techniques been developed for standardizing the translation of satellite measurements to surface soil moisture content (Price, 1980). The study of soil moisture estimation techniques is still progressing and a reliable technique has not yet been established. From satellite sensing, it is still difficult to precisely measure ground water contents, because complex environmental factors have to be considered. Exploring these topics is beyond the scope of this thesis. Therefore, our primary goal is developing an image segmentation technique for the acquired images.

The basic idea of our soil moisture estimation technique is based on Carlson's ground soil water content estimation model with the *triangle method*. When reviewing the related literature, we concluded that the triangle method is one of the most appropriate approaches to estimating ground soil moisture from optical satellite sensing. The triangle method uses the relationship between the surface radiant temperature and the vegetation index to estimate the surface soil moisture level. Full application of the theory requires extensive computation of weather and meteorological data. Thus, we attempted to simplify the triangle method to obtain rough (crude) soil moisture images.

A visible-red, a near infra-red and a thermal infrared band are essential for the soil moisture estimation technique. Section 3.2 explains the spectral characteristics and their properties. Section 3.3, explains the soil moisture estimation technique, the scatter-plot and the triangle method. Section 3.4 explains the mechanism and limitation of Oklahoma Mesonet soil moisture sensors.

3.2 Satellite Images and Characteristics of Spectral Bands

There are several sources of remotely sensed imagery that are currently easily acquired to compute the soil moisture. Table 3.1 summarizes the type of satellite and the equipped sensors.

Table 3.1: Summary of description of satellite sensors used for SM studies
(Source : Lillesand and Kiefer, 1996)

Platform:	NOAA11/12	Landsat4/5		SPOT 1-3
Sensor:	AVHRR	MSS	TM	HRV/MS
Orbit:	Near Polar	Near Polar	Near Polar	Near Polar
Resolution(m):	1,100	80	30,(120)	(10),20
Spectral Region	< ----------------- wave length (micro meters) --------------------------- >			
Visible				
Blue			[1]0.45-0.52	[1]0.51-0.73(10)
Green		[1]0.50-0.60	[2]0.52-0.60	[2]0.50-0.59
Red	[1]0.58-0.68	[2]0.60-0.70	[3]0.63-0.69	[3]0.61-0.68
Near Infra-Red	[2]0.73-1.10	[3]0.70-0.80	[4]0.76-0.90	[4]0.79-0.89
Mid Infra-Red		[4]0.80-1.10	[5]1.55-1.75	
	[3]3.55-3.93		[7]2.08-2.35	
Thermal	[4]10.3-11.3		[6]10.4-12.5(120)	

In order to apply the triangle method, we needed three bands: a visible-red, a near infra-red and a thermal infrared. The Landsat thematic mapper (TM) is superior to the AVHRR (Advanced Very High Resolution Radiometer) and the MSS (Multi-Spectacle Scanner) in terms of the spectral resolution. The TM sensor has all the necessary bands

31

required for the triangle method, so we selected the Landsat TM bands as our source imagery. Each of the spectral features and the wave lengths are shown in the previous table.
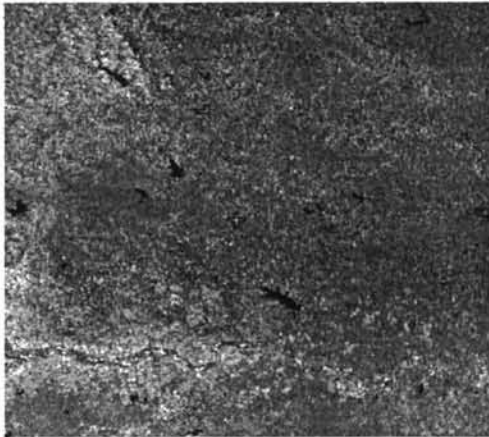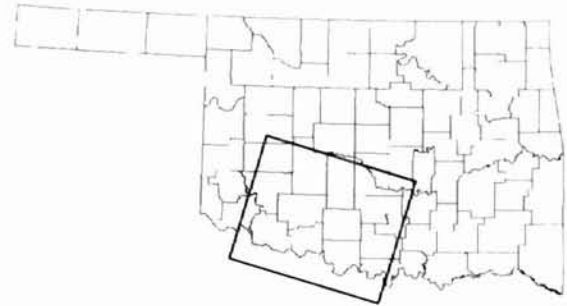
Fig.3.1(a) Entire TM image   Fig.3.1(b) The image region over Oklahoma

For our experiment, we have selected a 185 x 170 km region southwest of Oklahoma, which includes Little Washita basin. Historically this is one of the most studied areas for hydrological and meteorological experiments. Therefore, this area contains various ground truth sensing points, such as ARS Micronet and several Oklahoma Mesonet sites. Those sites are constantly monitoring local weather and surface meteorological parameters. The collection of soil moisture data was started in 1996 by the Mesonet. A total of nine sites are located over our satellite sensed region. We are expecting to obtain ground truth soil moisture data from the Mesonet sites. Currently the Mesonet sites are the sole data points for soil moisture ground truth measurement. But, the selection of this area has the potential to allow access to additional ground truth data acquired from related studies, such as soil moisture measurement from microwave sensors.

The satellite TM imagery for this study was acquired on a nearly cloud free summer day, July 25th 1997. The entire original image is shown in Fig. 3.1(a) and the related location is indicated in Fig.3.1(b) overlapping the area over a map of Oklahoma. Displaying the TM image using RGB bands, it is easily realized that the summer season of Oklahoma is teeming with healthy vegetation. We obtained summer season images, because the distribution of soil moisture tends to be more uniform in the winter season.

These three spectral bands, red, near infra-red and thermal infra-red TM bands are essential for this study. NDVI image is derived from the band-3 and band-4, and the scatter plot is drawn by the NDVI versus band-6. In Fig.3.2, we depicted the three bands and NDVI image from a 12 km square sub-region. The characteristics of each band are explained as follows.

Characteristics of Three Spectral Bands

This subsection explains spectral characteristics of each of the characteristics of the three bands. Fig.3.3 shows typical reflectance curves for three types of ground features: healthy green vegetation, brown bare soil, and clear lake water. The lines in the figure represent average reflectance curves and the pattern of the reflectance is applied to detect ground soil moisture.

TM band-3, visible red, locates $0.63 \sim 0.69\,\mu m$, is designed to sense chlorophyll absorption. Within the band length, chlorophyll strongly absorbs the radiated energy; this is the reason that our eyes perceive healthy vegetation as green in color. The band locates the first valley of the vegetation curve and is also useful in detecting artificial features over the image (Lillesand, 1994).

Fig.3.2   Three TM band images and NDVI image

Fig.3.2(a) TM Band3 Image

Fig.3.2(b) TM Band4 Image
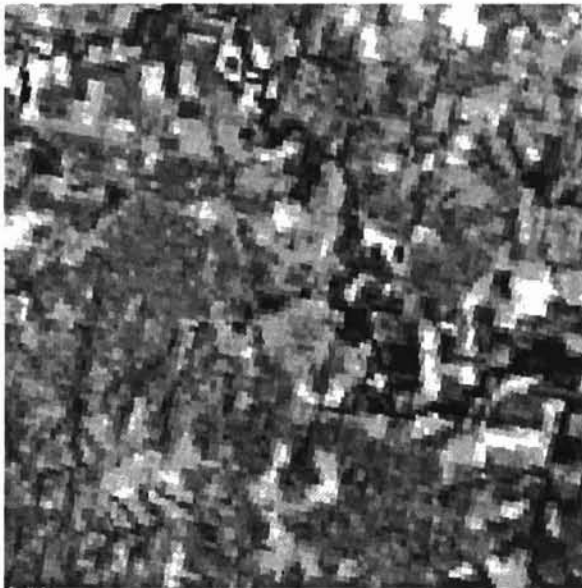

Fig.3.2(c) TM Band6 Image

Fig.3.2(d) NDVI Image

The man made features, such as roads and buildings give high reflection, which is shown in Fig.3.2(a). The red-band also tends to be affected by atmosphere, since the band senses water content in the air. As shown in Fig. 3.3, band-3 is located near the peak of the water reflection line.

Fig.3.3 Typical spectral reflectance curves for vegetation, soil, and water (Source : Lillesand and Kiefer, 1996)
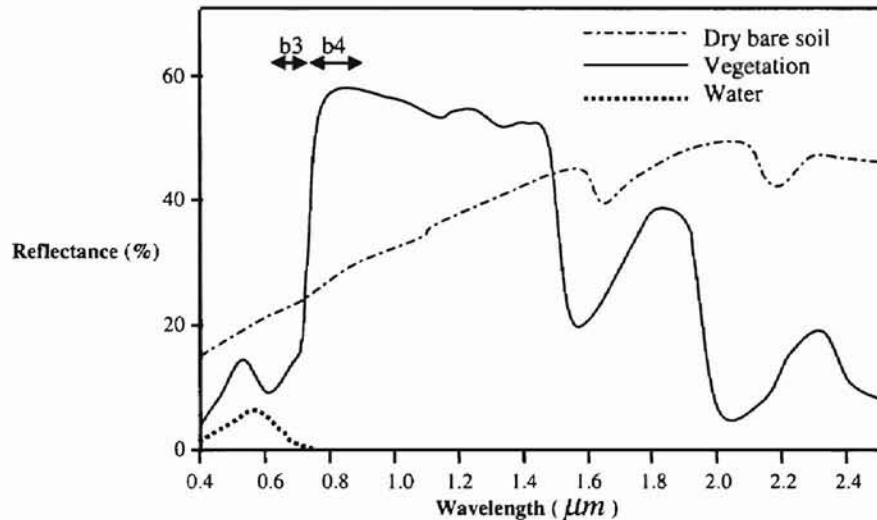
Band-4, is also called the near infra-red band and is located over the peak of the vegetation curve and after the end of water reflection curve. In this band, the reflection from roads and artificial features are not as noticeable as band-3, Fig. 3.2(b). Instead, the overall reflection from agricultural crops show the highest value. In Fig. 3.3, about $0.7 \, \mu m$, the reflectance of healthy vegetation increases rapidly. Plant leaves typically reflect about 40 ~ 50 % of the energy within the range. Thus, this band is typically used to analyze type of vegetation and to detect the vegetation level (Lillesand, 1994). The band is insensitive to water, so it is sometimes used to discriminate bodies of water from the image. In Fig.3.2(b), the bodies of water are shown at their lowest intensity (black).

From this TM band-4 image, the river and small lakes are clearly identified, whereas in the other bands they are not.

TM band-6 measures the amount of infra-red radiant from the surface and may also be called a thermal infrared band. This band is typically used to measure the distribution of surface temperatures. As we can expect, in Fig. 3.2(c) the bodies of water (the river) shows the lowest temperature (as black). The spectral resolution of band-6 is 120m, whereas the rest of the TM bands are 30m resolution. The coarse resolution makes the band-6 a blocky image, and therefore it has less distinct appearances than the other band images.

The normalized difference vegetation index (NDVI) is designed to measure global vegetation levels. This index is made by a simple combination of TM band-3 and band-4, the formula is shown as

$$NDVI = \frac{band3 - band4}{band3 + band4}.$$

Generally, the NDVI ranges between 0.8 for completely vegetated areas, 0.05 for completely bare soil, and near -0.5 for water bodies (Goward et $al.$, 1993). The index shows the amount of vegetation by using the characteristics of the two bands. Remember, band-3 is sensitive to artificial objects, but band-4 is not, and band-4 is sensitive to the vegetation but band-3 is not. Thus, the index can show the vegetation level with more contrast than the single band (Jensen, 1996). Fig.3.2(d) is an example of the NDVI image; the brightest regions (white regions) represent highly vegetated area, which are distributed along the bodies of water and are assumed to be grouped trees with thick leaves. The light gray area in the image represents cultivated crops. The darkest regions

are bodies of water, the man-made objects (such as roads) and bare soil fields. They are also clearly identified in the NDVI image.

3.3   The Soil Moisture Estimation Process

In the previous section we explained the characteristics of each band and the NDVI image. The second step for the soil moisture estimation in the triangle method is to draw the scatter plot. The scatter plot is drawn using NDVI versus band-6 and the plot indicates the relationship between the vegetation level and the radiant temperature. Fig.3.4 shows the typical distribution of a scatter plot. There are three clusters in the plot, a cluster of vegetation, a bodies of water and the bare soil. The vegetation cluster, which is the largest cluster, tends to distribute diagonally with a negative slope. This is due to the leaves having the ability of transpiration. This tends to preserve their temperature while receiving solar radiation.

Fig.3.4 The Scatter Plot
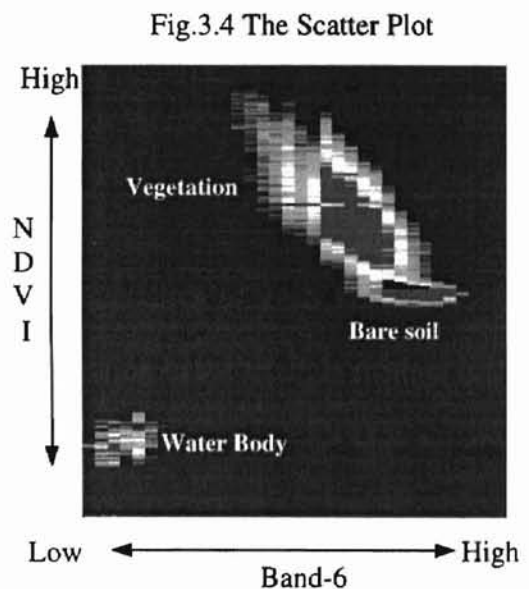
Typically, the distribution of bare soil forms a horizontal line in the scatter plot because of a constant NDVI value. During the daytime, the bare soil is heated by solar radiation and indicates the temperature depending on the amount of moisture content. Therefore, the radiant temperature of the soil can be a measurement of the surface soil moisture content. The third cluster in the plot represents bodies of water, which is usually located at the lowest NDVI with the lowest temperature.

37

The Triangle Method

The triangle method is a soil moisture estimation technique using the scatter plot. The name of the triangle method is derived from the shape of the scatter plot. The method assumes that soil moisture is mostly dry, on the right edge, and mostly saturated, on the left edge, as in Fig.3.5. The triangular shape can be interpreted as the areas with the highest vegetation indicating a higher NDVI with lower temperatures. Thus, for a given NDVI, relatively high temperatures correspond to low amounts of soil moisture. Using this relationship, we can map the moisture level.

Fig.3.5 The Triangle Method
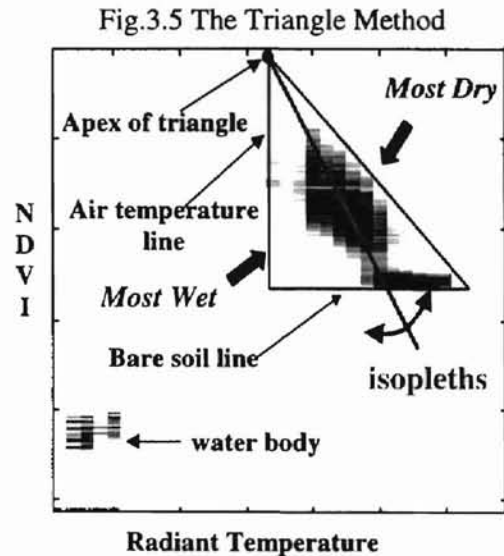
According to the Carlson's study, the *isopleths* are those lines that have the same soil moisture level and they are derived from the SVAT (Soil-Vegetation-Atmosphere Transfer) model, which was created by analyzing the extensive relationships of local weather and meteorological parameters. Once the isopleths are drawn over the scatter plot, we can interpret the distribution of moisture from the plot. A very similar approach has been studied by Price (Price, 1990), and both Carlson and Price have shown that the method has the potential to estimate surface soil moisture level.

If directly applying the triangle method to a large region, we would have to consider the local weather and meteorological differences. This requires extensive

collection of various local hydrological parameters with additional computations. In order to minimize local weather influences and in order to simplify the soil moisture estimation model, we focused on relatively small regions of about 12km x 12km. In other words, we assumed these local climate variations could be minimized using relatively small regions. Hence, using the fundamental relationship between the isopleths and scatter plot, and
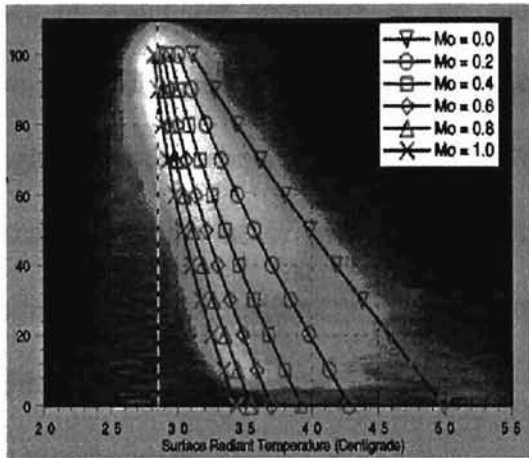
Fig. 3.6 A scatter plot and overlapped isopleths

The vertical axis shows normalized NDVI and the horizontal axis shows surface radiant temperature in centigrade. Once scatter plot is drawn isopleths are overlapped on the graph. The isopleths are derived from the SVAT model. In the plot, the moisture level is shown as M_o, $M_o = 0$ represents most dry line and $M_o = 1.0$ represents most wet line.

Source : NASA-EOS Report (1995, Carlson[2])

using a relatively small region, we attempted to draw simplified isopleths over our scatter plot. In theory, the isopleths are drawn with a slight curve as shown in Fig. 3.6. But, we have assumed the isopleths are linear and equally spaced in slope from the most dry side to the most wet side as shown in Fig.3.5. Starting from a drawing of a scatter plot, the major steps of our triangle approach are shown as follow.

Step 1: Locate a vertical line, which is the end of the vegetation cluster. Theoretically, this line can be substituted as an air temperature line. Locate the bare soil line, which is the horizontal line.

Step 2: Locate the triangle apex, which should be the end of the vegetation cluster and on the vertical line. In general, the apex of the triangle is chosen at the total vegetation point and at the temperature that includes the most pixels within the triangle.

Step 3: Assume that the dry line has minimum moisture and the wet line has been saturated by moisture. Swing straight isopleths from the dry side to the wet side, then translate the moisture level onto a soil moisture image map. We used 255 isopleths to draw the 255 graylevel moisture map. During this step, the bodies of water are recorded as the most wet region. A soil moisture image derived from the triangle method is shown in Fig.3.7. The wettest regions are shown as bright pixels and the dry regions as darker pixels. The river and the neighbor areas are adequately indicated as the most moist region.

Fig.3.7 The Soil Moisture Image
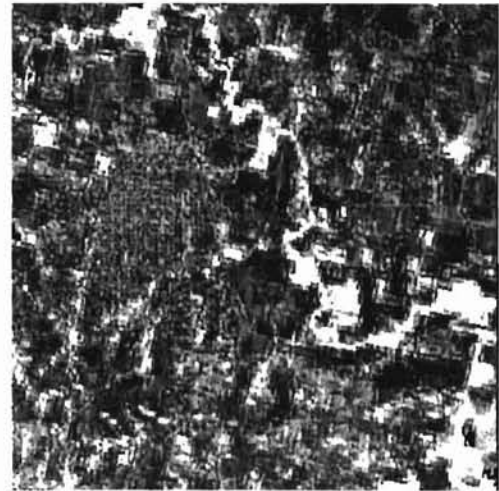
3.4   Mesonet Soil Moisture Sensors

In the last part of this chapter, we would like to briefly describe soil moisture sensors in the Mesonet sites. The Oklahoma Mesonet started recording the soil moisture data in 1996. There are two types of soil moisture sensors in the Mesonet. One is called heat dissipation matric potential sensors, and the other is called the Time Domain Reflectometry (TDR) sensors. The TDR sensor's design is based on a manual device, so there is not an automated stream of data. Therefore, the data from the automated heat dissipation sensors are the only possible way to collect ground truth data for soil moisture measurement from the Mesonet. Up to now, nine heat dissipation sensors are located within our entire 185x170 km region, and the data are recorded at 30 minute intervals. The sensors are equipped with heaters and

they measure two points of temperature, before heating and after heating. Then the potential wetness of the sensing point can be estimated from the temperature difference ΔT. According to the Mesonet, the heat dissipation sensor is described as follows.

"The sensors are basically a thermocouple and a heater imbedded in a needle encased in porous porcelain. The ambient temperature is first measured, then the sensor is heated twenty seconds, then the temperature is measured again. Depending on how much heat is absorbed by the soil, which will influence the two difference in two temperatures. Due to the high capacity of water with respect to soil, it will be difference in the temperature change depending on how much water is in the soil"(Basara, 1997). Obviously, this sensor does not directly measure the amount of soil moisture, and the ΔT is influenced by the soil type. The data require a calibration in order to translate the ΔT to correspond to the gravimetric soil moisture level. This study is ongoing (Basara and Elliott 1997).

As a test, without using calibration, we simply compared each set of ΔT Mesonet streamed data to the corresponding soil moisture image. Following the basic relationship, we could find some correlation between the two data: the larger the ΔT, the drier. When we compared both data (our estimation and the Mesonet data) only a slight correlation was observed, $r^2 = 0.43$. There are possibly two reasons for this. First, each ΔT should be calibrated by considering the soil type, and second, the Mesonet measure pin-pointed the local data, but these satellite records region-averaged data (spatial resolution). Without using any calibration or having a fine ground truth measurement, there will be large differences between the two data. To obtain ground truth data from another source, a microwave measurement can be a potential approach. The study on microwave sensing is progressing over the Little Washita area of Oklahoma.

41

3.5 Summary

This chapter described the mechanism and process of a soil moisture estimation technique following the triangle method. The derived soil moisture image from the triangle method is shown in Fig.3.7. Visually, the soil moisture image has a reasonable distribution of soil moisture. The only pitfall in this process is that we do not have reliable ground truth data to verify the derived soil moisture images. Research on soil moisture over the region is progressing.

On the other hand, our main goal for this thesis is to develop an advanced image segmentation technique. We are going to start the process using the soil moisture images. The following chapter provides analysis of the image segmentation technique. Starting from the definition of image segmentation, we will introduce the best segmentation technique for the soil moisture images.

Chapter 4. The Watershed Segmentation and Region Merging

4.1   Introduction

This chapter proposes a possible solution to the two major weak points of the watershed (WS) algorithm. In the actual image segmentation, large computational cost and over-segmentation are two common disadvantages of the algorithm. In this thesis, we first want to show reasonable solutions toward these two issues of the WS.

The first section, section 4.2, explains the mechanism of the WS segmentation algorithm. In order to reduce the computational cost, we applied the concept of the image pyramid to form a multi-resolution watershed pyramid. By applying the multi-resolution image segmentation approach, we were able to attain faster computation and region scalability.

Finding a reasonable region growing and clustering technique is a key step to yield sound segmentation results. Conventionally, region merging is implemented in a heuristic manner. Here, we propose a well-motivated region clustering technique by applying a variational technique. The first step of the variational technique is the formulation of the energy function. Once the equation is formulated, regions are merged according to their energy levels. This merging scheme is advantageous over the conventional scheme due to the ability to control region scale. Additionally, the equation enables us to measure the segmentation results. Measuring segmentation quality is an essential task, because it is one way to measure the quality of the complex soil moisture segmentation results. The details of the variational approach and the merging algorithm are fully explained in section 4.6.

4.2 The Watershed Segmentation Technique

The WS segmentation technique is a powerful image segmentation tool, which always yields thin and closed contours. But, large computational cost has been a major disadvantage of the algorithm. This section explains the mechanism of the algorithm, then eventually associated costs are analyzed. In Section 4.3, the multi-resolution WS is introduced as the remedy to the large computational cost. First, we will explain the steps of the WS segmentation.

Flow of the WS algorithm

The first step of WS is making a gradient magnitude of the original image $|\nabla I|$. Let us consider the I to be a two dimensional grayscale image which has digital values from 0 to 255. Using x and y-coordinates to represent the two dimensional space, we have

$$\mathbf{I} : (x, y) \rightarrow \{0, 1, 2, \ldots, 255\}, \tag{1}$$

$$\forall\ x \in I,\ y \in I.$$

The gradient magnitude of the original image $\mathbf{I}$, $|\nabla I|$ is given by

$$|\nabla I(x, y)| = \sqrt{\{I(x, y+1) - I(x, y)\}^2 + \{I(x, y) - I(x+1, y)\}^2}. \tag{2}$$

Next, the gradient magnitude image is slightly blurred. The blurred image $\mathbf{BI}$ is formed by applying (convoluting) a Gaussian kernel $\mathbf{G}$ to the $|\nabla I|$. This process is necessary, because the original integer value of $|\nabla I|$ provides poor representation of a smooth surface, $i.e.$, each point in the image $\nabla I(x, y)$ should have a locally unique value. This process eliminates the plateaus in the image and simplifies the process to identify local maxima and minima. This second process is shown as

$$\mathbf{BI} = \mathbf{G} * |\nabla I|. \tag{3}$$

44

In the third step, all local minima should be identified and all catchment basins are labeled. Each pixel $\nabla I(x, y)$ is compared with its eight spatial neighbors. If the value of all of the neighbors are greater than the center pixel, the pixel is identified as a local minimum. Thus, an element $M(x, y)$ is said to be a local minimum

$$\text{if } M(x, y) < p(x_0, y_0),$$

$$\forall (x_0, y_0) \in N(x, y),$$

where $N(x, y)$ represents spatial neighbors of the pixel at row x and column y in eight connectivity.
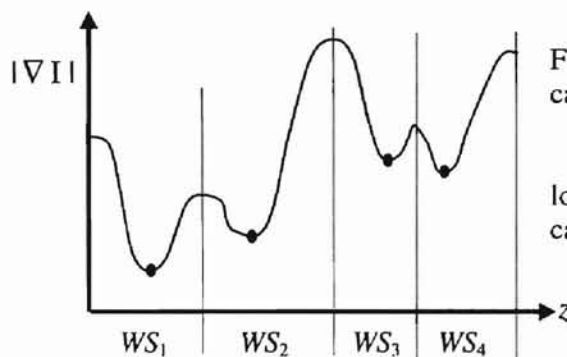
Fig.4.1 The location of minima and the catchment basins in one dimensional example

This one dimensional example shows the location of minima at the black dots and the catchment basins as WS_1 - WS_4

Once all of the local minima in the image are identified, these minima are assigned a unique identification (ID) number. The ID is used to label the catchment basins. In our WS, the minimum following algorithm is used for the catchment basins labeling process, which is discussed bellow.

The Minimum Following Algorithm

Remember that watersheds are defined in terms of the drainage pattern of rainfall. Regions of terrain that drain to the same local minimum are defined as the same watershed (catchment basin). The same analysis can be applied to an image by viewing the gradient magnitude as height. The gradient magnitude of the image, ∇I is used to find the direction of the drainage.

45

In the image **BI**, each point of *BI*(*x*, *y*) is examined by seeking the lowest valued neighbor until it merges into one of the local minima M_i or an already labeled catchment basin. This scheme is called the minimum-following algorithm, because each element constantly seeks lower altitude in the image terrain. Once the image element drains to the catchment basin, it is labeled with the same ID number as the local minimum. In Fig.4.1, there are four local minima, and four catchment basins which have been formed (grouped) according to the labeling process.

Once all pixels in the image have been associated with their respective minima, the output image has the watershed patterns (grouped regions). We will define a function *WS* that represents the minimum following algorithm. Then the watershed image **W** can be defined as

$$\mathbf{W} = WS_d\,(\,\mathbf{G} * |\nabla I\,|\,), \tag{4}$$

$$WS_d \equiv \{\,(x, y) \Rightarrow WS(x, y) = d\,\},$$

where *WS*(*x*, *y*) is the watershed labeled region and *d* is the region ID number. The WS segmented image **W** yielded a new independent image. In (4), WS_d represents all of the elements in region-*d* that have the same catchment basin number *d*.

The WS boundary detection is the last step of the fixed resolution watershed. The watershed boundaries are detected by searching the difference of the WS region number. The WS edge map image, **E,** can be drawn by detecting and recording the region differences over **W**. If we assign "1" for the location of boundaries and assign "0" for the rest of the area, this process can be shown as

$$E(x, y) = \begin{cases} 1 & \nabla W(x, y) > 0 \\ 0 & otherwise \end{cases}. \tag{5}$$

In Fig.4.1, an original one dimensional signal is divided into four regions, and the dotted lines represent the edge locations. Unfortunately, the above fixed-resolution WS requires large computational costs when it is applied to a more practical image size. Hence, we introduced the concept of multi-resolution WS for the reduction of the computational costs.

4.3   The Multi-resolution Pyramid and the Watershed

If the fixed-resolution watershed algorithm is directly applied to the original image size, there will be large computational expenses. The concept of the image pyramid is the key to solving this issue. A flow of the multi-resolution watershed (MR-WS) is shown in Fig.4.2. The concept behind the multi-resolution pyramid is to create a scale space where only the most significant features appear at the coarsest representation. The multi-resolution watershed pyramid is introduced and demonstrated by Gauch and Pizer (Gauch and Pizer, 1993). In contrast to their approach, however, we applied the watershed

Original Image

⇩

Construction of Image Pyramid

⇩

Root Level Selection

⇩

WS segmentation at the Root level

⇩

WS Edge Propagation

Fig.4.2 Flow of the MR-WS

at a coarse root level and propagated the edges back to finer pyramid layers without directly performing the WS on each layer.
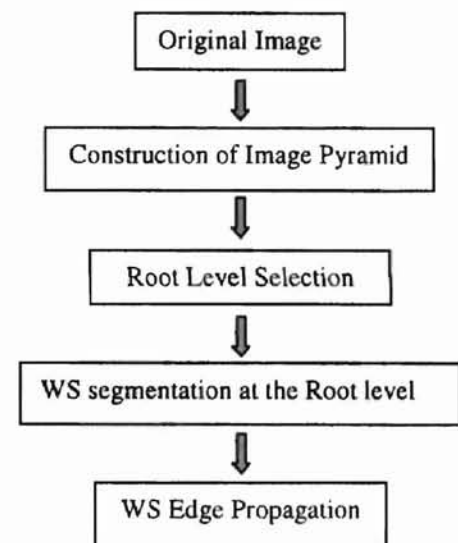
In order to construct a morphological image pyramid, the original image was sequentially applied with open-close filtering and sub-sampling. The process can be denoted as

$$\mathbf{I}_L = [(\mathbf{I}_{L-1} \circ \mathbf{K}) \bullet \mathbf{K}]_{\downarrow 2} \qquad (L=0,1,\ldots, n.). \tag{6}$$

When $L = 0$, $\mathbf{I}_0$ represents the original image and $[\cdot]_{\downarrow 2}$ represents down sampling by a factor of two. $\mathbf{I}_L$ is referred to as the *parent* layer and $\mathbf{I}_{L-1}$ referred to as the *child* layer in the pyramid. With one-of-two down-sampling in both dimensions, each dimension becomes half of the original size.

In (6), $(\mathbf{I} \circ \mathbf{K})$ and $(\mathbf{I} \bullet \mathbf{K})$ represent a morphological opening and closing operation by structuring element $\mathbf{K}$, respectively. The open-close operation works as a low pass filtering, smoothing the image and erasing insignificant features. The open-close filtering has been assigned because it produces the least graylevel bias compared to the individual open or close operation. The morphological filters are known to be superior to linear filters in terms of edge localization and feature preservation (Morales and Acharya, 1995). The open-close filtering and sub-sampling steps are applied to all the pyramid layers until a pre-selected root level is formed.

The Multi-resolution WS and New Edge Linking Process

Once the watershed algorithm is applied at the root level L, each image element of $\mathbf{W}_{L-1}$ has to be linked to an element in $\mathbf{W}_L$. All elements on the root level are linked to a finer image layer. This process is shown as

$$\mathbf{W}_{L-1}(x_0, y_0) = \begin{cases} \mathbf{W}_L(x, y) & \textit{if } |\nabla \mathbf{W}_L(x, y)| = 0 \\ \textit{undefined} & \textit{if } |\nabla \mathbf{W}_L(x, y)| \neq 0 \end{cases}. \tag{7}$$

for all $(x_0, y_0) \in \mathbf{C}(x, y, L)$,

where $\mathbf{C}(x, y, L)$ represents the children of element (x, y) at level L-1.

In (7), if $|\nabla \mathbf{W}_L(x, y)| = 0$, implying that no change in the watershed label exists in that neighborhood, we can say that the label for the children of $\mathbf{W}_L(x, y)$ is *known* to be

equal to the label of $W_L(x, y)$. But, if $|\nabla W_L(x, y)| \neq 0$ then the label of the children in question is undefined. Then, to define the label the watershed is applied *only* for the undefined elements. The undefined pixels are usually the WS boundaries of the parent layer. Therefore, the final step in linking level $L\text{-}1$ to level L is to apply the watershed algorithm on the undefined pixels (propagated boundaries) of $W_{L\text{-}1}(i, j)$.

$$W_{L-1}(x_0, y_0) = WS[BI_{L-1}(x_0, y_0)], \tag{8}$$

$$\forall\ (x_0, y_0) \in \{\ |\nabla W_L(x, y)| \neq 0\ \},$$

where **BI** is the same as defined previously.

Edge propagation

$W_{L\text{-}1}$

W_L

WS is performed only at the boundaries

After the WS, borders become thin again
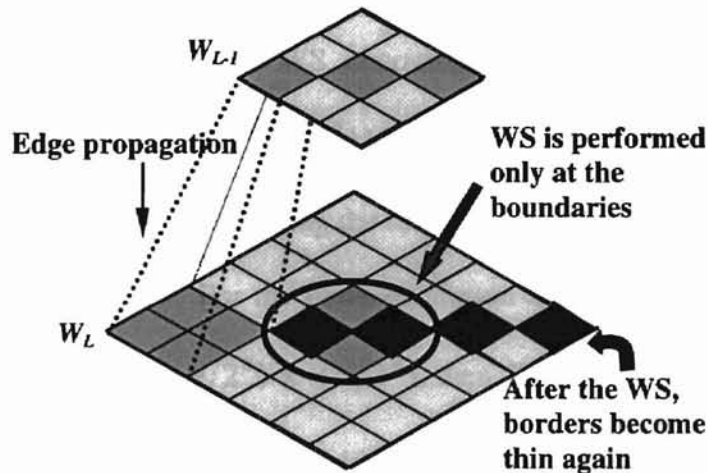
Fig.4.3 **An illustration of our proposed boundary propagation process.** Once boundaries are propagated from layer $W_{L\text{-}1}$ to W_L, the WS is performed only at the boundaries (gray pixels). Extensive computational cost can be reduced through this approach. The darkest pixels are the new WS boundaries that emerged by this process.

This linking process continues, level by level, and terminates when the level corresponding to the original image resolution is accomplished. Since the image pyramid structure insures the causality of watershed boundaries, no boundaries can appear in level $L\text{-}1$ that do not exist in level L. This process is illustrated in Fig.4.3 and shows why our multi-resolution approach reduces computational cost. In each edge propagation step, the WS is applied only on the propagated boundaries. This algorithm dramatically improves

49

the computational expense. The explanation and computational example are shown as follows.

Computation Costs in the Multi and Fixed-resolution Watershed

Generally, the multi-resolution algorithm decreases the computational cost of the watershed segmentation by an order of magnitude (of the root level). Assuming the computational cost on a comparison between elements is equivalent to an addition operation, the cost of performing the full-resolution watershed on an NxN image is: $3N^2$ adds and $2N^2$ multiples for the gradient magnitude ∇ operation, $8(G \cdot N)^2$ adds and $9(G \cdot N)^2$ multiplies for convolution with GxG size of Gaussian kernel, and $10N^2$ adds to perform the WS operation. This means that the full-resolution watershed algorithm requires $(13+9G^2)N^2$ addition operations and $(2+9G^2)N^2$ multiplication operations, without including the computational cost of pre-filtering.

For the multi-resolution algorithm, the watershed is applied at a root level R of size $(N/2^R)$ x $(N/2^R)$, then linked to the finer levels of the pyramid. The cost of constructing the pyramid using an open-close filter with a kernel, size KxK, is $4K^2\sum_{L=0}^{R-1}(N/2^L)^2$ adds. Now assuming there are E_R elements in level R which represent watershed boundaries, the watershed has to be performed on $4E_R$ elements to link level R to level R-1. Approximately, this link produces $E_{R-1} \approx 2E_R$ elements in level R-1 because connectivity has been maintained. The resulting computational cost of linking the multi-resolution watershed is $(13+9G^2) \cdot 4\sum_{L=0}^{R-1}2^L E_R$ adds. The computational cost comparison

for the actual image segmentation between the fixed-resolution WS and the multi-resolution WS is shown as follows.

For more intuitive understanding, we compared the computational expense of the multi and fixed-resolution WS experimentally. In this experiment, a 512x512 original sized image, a 3x3 Gaussian matrix, and the 3x3 open-close filter were used. Without using the image pyramid (fixed-resolution watershed), on average it took about 19 minutes (using a Unix Workstation) to process the watershed segmentation on a 512x512 soil moisture image. By applying the multi-resolution watershed, at root level two (image size = 256), it took about 1.6 minutes and at root level three (image size = 128), it took about 29 second for the watershed segmentation. Further details and comparisons of the computational cost on the soil moisture images are shown in Chapte-5.

4.4   Region Merging Techniques

Region merging is the key to post-processing the watershed segmentation, because the watershed produces an over-segmented image. Usually, it is difficult to obtain a reasonable segmentation without applying some kind of region merging. Therefore, the success or failure of the final segmentation depends upon the region merging technique.

In this section, three region merging techniques are explained, two conventional and one new merging technique. The first conventional technique is based on a single-linkage region growing scheme. The second is the single-linkage region growing scheme with recursive region merging. This algorithm improves upon the first algorithm by utilizing the concept of clustering hierarchy. For the third approach, a new and more

sophisticated region merging technique is introduced, - the stepwise merging optimization approach combined with the variational technique. The following table summarizes the characteristics among the conventional and new merging techniques. The mechanisms of each region merging technique are explained in order in the following section.

Table 4.1 Conventional and New Merging Schemes

Merging Technique	Similarity criterion	Hierarchy	Category
Single Linkage	Averaged Region Intensity	No	Conventional
Single Linkage Recursive	Averaged Region Intensity	Yes	Conventional
Variational Model	Weighted Region Variance	Yes	New

4.4.1   Single Linkage Region Merging Technique : Conventional

In the single-linkage region merging technique, the region similarity is measured by a fixed threshold value. Using the threshold value (clustering criterion), adjacent region similarities are measured. In this scheme, the graylevel of the each WS mosaic region is compared to the region clustering criteria. Once the WS is applied to the original image, it segments the original image into small (over-segmented) WS regions. Then, the WS mosaic image is formed averaging the WS regions that correspond to the original image. Thus, the value of the mosaic region M_d for region d is defined as

$$M_d = \frac{1}{n_d} \sum_{(x,y) \in WS_d} I(x,y), \qquad (9)$$

where n_d is the size (number of pixels) of the region d, and I is the original image.

According to this merging algorithm, regions are merged if the adjacent mosaic graylevel is less than the criterion. Once regions are merged, the mosaic value of the merged region is updated according to (9). This process is applied to all regions over the

image and the region merging is terminated when no more regions can be merged at the given threshold value.

In this scheme, the segmentation is controlled by the threshold value and the root level selection. Conventionally, the threshold value and root level are chosen to segment desired target objects and these parameters are obtained in a heuristic manner. There is no standard to selecting the threshold value and the root level. Additionally, this scheme is biased in the merging order, because the merging progresses from one corner of the image to the other.

The application example of this scheme to a soil moisture image is shown in Fig. 4.4, and the original image is shown in Fig.4.4(a). The region includes a river which is considered a high moisture content area, and is depicted as white in the image. In this segmentation experiment, three root levels – root level one, two and three are used. Four levels of threshold values, zero, five, ten, and fifteen are applied to each root level. By comparing these three images, Fig.4.4(b), 4.4(f), and 4.4(j), the relationship of the region scalability and the root level selection is clearly understood.

A selection of a low root level (Root=1) will make fine scale regions, and the fine features (ex, the river) are still preserved as seen, in Fig.4.4(b). But, in root level two and three, Fig.4.4(f) and Fig.4.4(j), the river regions have been merged (destroyed) to other regions even before the start of the region merging process. From the results, it is understandable that the selection of root level two and three are inappropriate for the image segmentation. Now, let us look at the results of three segmentations from root level one. When threshold $T=15$ is applied at root one, Fig.4.4(e), the river is merged to other regions.

Fig.4.4 SM segmentation results from Single Linkage Region Merging (Fixed Threshold)
Original WS Mosaic Image
(a) Root = 0, Root size = 512
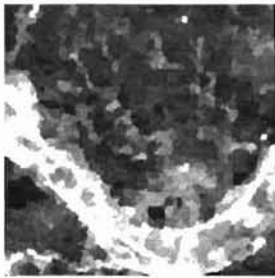
Root =1, Root size = 256
(b) *T*=0, *R*=2151   (c) *T*=5, *R*=475   (d) *T*=10 , *R*=281   (e)*T*=15 , *R*=233
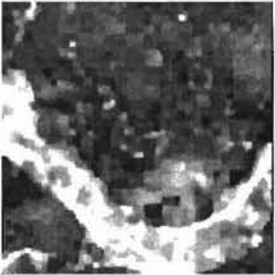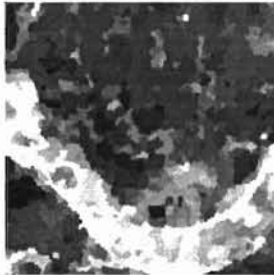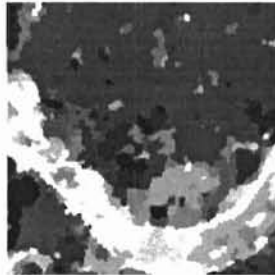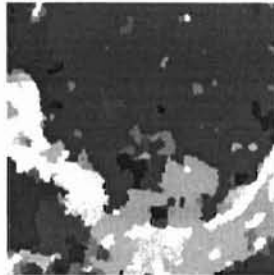
Root=2, Root size = 128
(f)*T*=0, *R*=329   (g)*T*=5, *R*=265   (h) *T*=10 , *R*=158   (i) *T*=15 , *R*=93
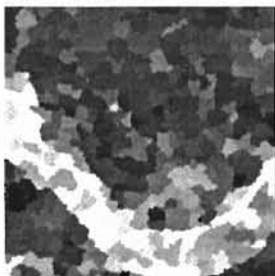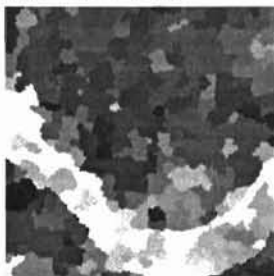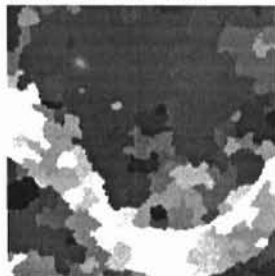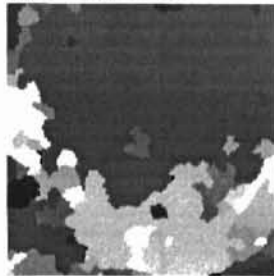
Root=3, Root size = 64
(j)*T*=0, *R*=119   (k)*T*=5, *R*=73   (l) *T*=i0, *R*=39   (m) *T*=15, *R*=30
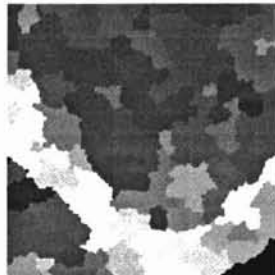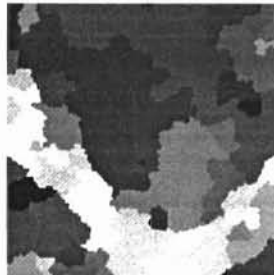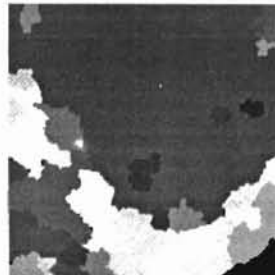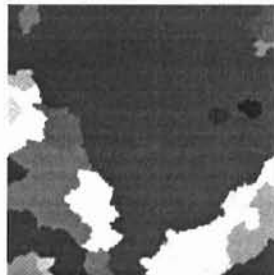
(*T* denotes the threshold value, and *R* denotes the number of regions in the image)

Yet, the merged results show many small regions (shown as specs), which is an example of a poor segmentation. Because of lack of the region scalability, the image has (mix) small regions and large regions. Fig.4.4(e) still has more than 200 regions, and even the river was merged! We can even visually recognize the weakness of this merging algorithm, because we want to segment (classify) fewer regions *and* preserve finer features, such as the river. And in a latter section, we will measure these segmentation results using an appropriate measuring scale.

Unfortunately, this merging scheme is too awkward to apply to these complex soil moisture images. In the following section, we will introduce the modified version of the merging scheme – the single linkage region merging with recursive threshold algorithm.

4.4.2 Single-Linkage Region Merging with Recursive Threshold : Conventional

As we have seen, the first merging technique was inadequate for the SM image segmentation. The single linkage region merging with recursive threshold technique, Fig.4.5, has been developed to improve the weakness of the previous merging scheme (Meyer, and Beucher, 1992). This merging method can be applicable to more complicated and low contrast images. Here the threshold is not fixed;
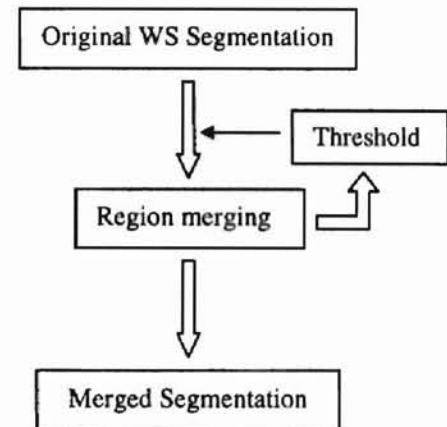
Fig.4.5 Flow of the Recursive Thresholding

it is gradually increased. Using the merging mechanism, regions are merged from similar regions, so distinguished regions are preserved until the last merging stage. The composite graylevel of each mosaic region is used for the merging criterion just as it was in the previous merging scheme. But in this algorithm, the most similar pair of regions is

selected from the entire WS mosaic regions and merged. When no regions can be merged at a given threshold value, the threshold value is incremented slightly and the merging continues until a desired number of regions are obtained.

One advantage of this merging scheme is that it has an ability to yield the desired number of segments. Also, merging order has no bias because the merging is progressed from the most similar regions. This merging order makes a hierarchy of region merging (merging hierarchy), whose mechanism is explained below.

Hierarchy of the Region Merging

Starting from an over-segmented watershed mosaic image, a hierarchical merging structure represents the merging order in the segmentation structure. In this scheme, the regions are merged one by one according to the merging criterion. The merging hierarchy can be visualized using a tree

Fig.4.6 An illustration of Tree Diagram
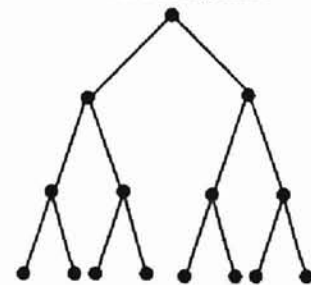
diagram, which is shown in Fig.4.6 (Beaulieu, and Goldberg, 1989). In the diagram, each node represents a region and the links between the nodes indicate the paths of the merging. These regions, at the lower level, are clustered in the early merging stages and form a higher level of segments. The hierarchical levels can be related to the resolution. Thus the merging hierarchy also represents the region scalability.

This algorithm can be considered as a reasonable merging scheme, but one disadvantage is that it does not consider the region size in the merging process. Small, but extremely high or low intensity regions do not merge with neighbors and are left until the last merging stage. This is an issue in the controlling of region scalability. Using Fig.4.7,

we show the results and illustrate the weakness of the merging algorithm. The top-left image Fig.4.7(a) is an original over-segmented WS image – the same image as the previous example. Fig.4.7(b) is the segmentation result at the number of regions = 100, while Fig.4.7(c) is the segmentation result at the number of regions = 30.

Fig.4.7 SM segmentation examples from Single Linkage Recursive Threshold
Root level = 1, root size =256

| (a)Original SM mosaic image | (b) Number of regions = 100 | (c) Number of regions = 30 |

| (d)Original SM mosaic image | (e) Number of regions = 50 | (f) Number of regions = 30 |
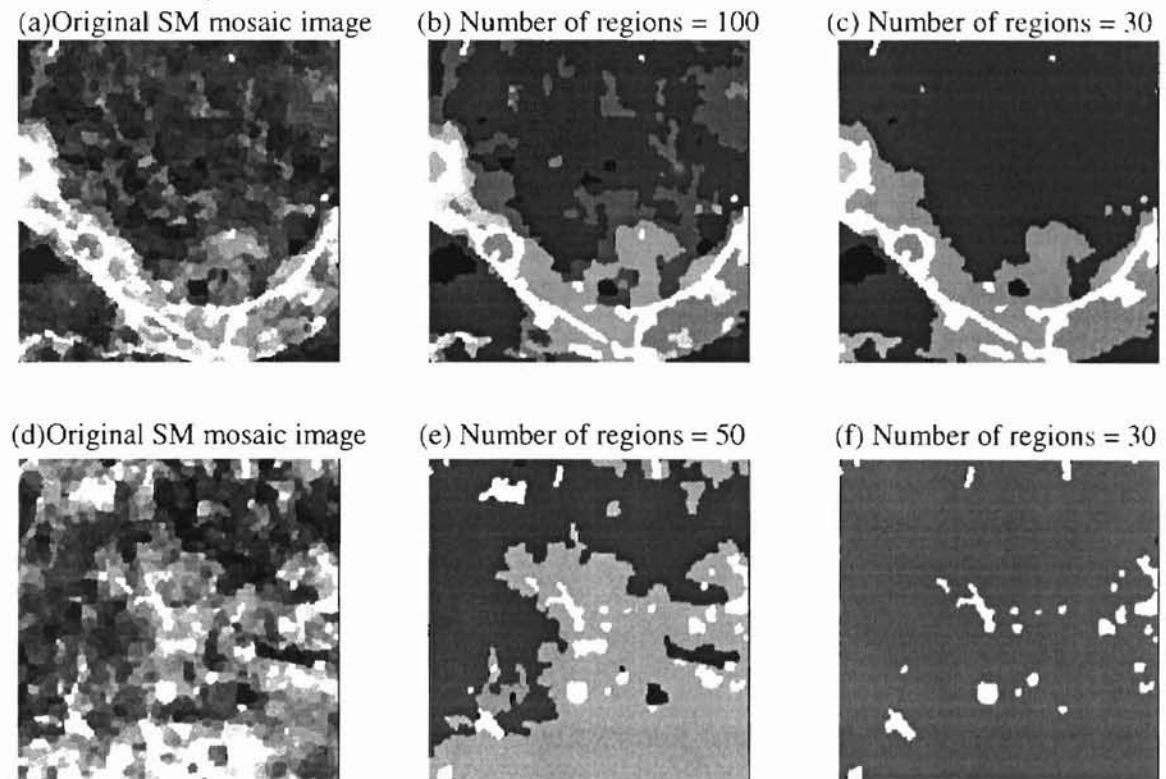
The second row of Fig.4.7 shows the segmentation results from another SM image. Starting from an over-segmented WS image, Fig.4.7(d), the segmentation results are shown in Fig.4.7(e) and Fig.4.7(f) at the number of regions is 50 and 30 respectively. From the segmentation examples, improvements can be recognized and compared to the previous merging scheme. But, this segmentation scheme still merges homogeneous regions too rapidly. Large regions of similar graylevel are merged into one region, while small scale regions remain unchanged as shown in Fig.4.7(e) and Fig.4.7(f). Therefore,

this algorithm also lacks region scale controllability. Our goal is to segment regions by forming uniform scale regions yet minimizing the loss of original SM distribution.

In order to solve this dilemma, a new merging method is introduced - the stepwise optimized clustering algorithm using the variational technique. This new merging algorithm resolves the weak points of the conventional (previous) merging algorithms. One of the major improvements of this algorithm is the *weighted- regions variance* is used for the similarity measurement. This technique is quite appropriate for the segmentation of soil moisture images, because the images tend to show lower contrast and the graylevel varies gradually. Also, this algorithm considers the region size during the merging process. Additionally, using the concept of image energy, we can evaluate the segmentation quality. Being able to measure and evaluate the segmentation result is important. In the following section, a new concept, the variational technique with an energy equation is introduced.

4.5   The Variational Technique

The variational technique is a new approach compared to the conventional region merging schemes. Using the variational technique, we formulate an energy equation, then by solving the equation, we segment images. So, formulating the equation is the key step in the variational model. First, we have to translate the properties of the image segmentation to form an appropriate function.

In our image segmentation (region merging), we focused on two terms – the number of segmented regions and region smoothness to form our energy equation. The smoothness and the number of regions represent opposite segmentation statuses. If a

segmented image has fine scale(large number of regions), each region will have uniform (smooth) elements in the region. On the other hand, in a coarse segmentation (a few number of regions), inhomogeneous (unsmooth) elements are in each region. Therefore, the region smoothness and the region scale (the number of the regions) are considered in forming our image segmentation function.

Another advantage of the function is that the segmentation quality can be measured according to the energy level. Having an appropriate measurement to evaluate the merging quality is important. In particular, SM images are complex and the regions tend to have uniform graylevel, which makes it very difficult to compare the segmentation results visually. Without depending on the image type (simple to complex), we can measure the quality of segmentation from various region merging schemes. The process of our energy equation formulation is explained in the following section.

4.5.1 The Energy Function Formulation

As we mentioned previously, we are focusing on the region smoothness and the number of regions. Our energy function, or cost function, describes the relationship between the two terms. The first term of the energy function is region variance. We measure region smoothness using the variance of the region and it is weighted according to the size of the region. The weighted variance (or sum of variance) of a region i is defined as,

$$\text{Weighted Variance } (SOV) = S_i \cdot Var(O_i). \tag{11}$$

S_i represents the size of the region O_i, and $Var(\cdot)$ denotes variance of the region O_i. This term measures smoothness of the region while also considering the region size, and is often called the *data term* in the energy function. The next term is the cardinality of the

segmentation. *Card(O$_I$)* denotes the number of segments in the entire image, *I*. This term

is called the *scalability term* or *cardinality term* and represents the energy of the region

scale.

Total energy is given by combining the two terms - the variance and the

cardinality term. The total energy of an image is given by the summation of the weighted

variance and the cardinality of the image.

$$E_{image} = \sum_i S_i \cdot Var(O_i) + \lambda(Card(O_I)). \qquad (12)$$

Thus, the total energy measures the regions' smoothness and the number of regions at the

given λ. In (12), the λ is called a scalability parameter, which controls the scale of the

regions. The physical meaning of λ is the cost for merging. The equation (12) can be

seen in Morel (Morel and Solimini, 1994). But in our merging scheme, λ starts from a

low number, then regions are merged from the most similar regions, and then λ is

gradually and monotonically increased until desired number of region is obtained.

The following example explains how the energy function works by providing a

simple illustration, assuming there are only two regions, region *i* and *j*. This example is

convenient, because we always merge a pair of regions at once in our merging scheme.

According to the above equation, we compute two energy functions before merging and

after merging according to the equation (12).

$$E_{before\ merge} = S_i \cdot Var(O_i) + S_j \cdot Var(O_j) + 2\lambda.$$

$$E_{after\ merge} = S_{i\cup j} \cdot Var(O_i \cup O_j) + \lambda.$$

The data-energy increases when the regions merge, *i.e.*, data-energy in two regions before

merging are lower than after the merge. This can be shown by a example via a simple one

dimensional matrix as shown below,

$M_A = [9\ 8\ 6\ 5\ 4\ 3\ 2\ 2\ 3\ 4;\ 4\ 3\ 2\ 2\ 1\ 1\ 1\ 2\ 3\ 4] = [M_1, M_2]$.

Assuming M_1 and M_2 are independent WS mosaic regions.

Fig. 4.8(a)   Fig. 4.8(b)   Fig. 4.8(c)

Fig. 4.8(a) is a graph that indicates the elements of M_1 and M_2. Fig 4.8(b) shows region M_1 and M_2 before merge. Fig 4.8(c) shows the merged pattern after the two regions are merged.
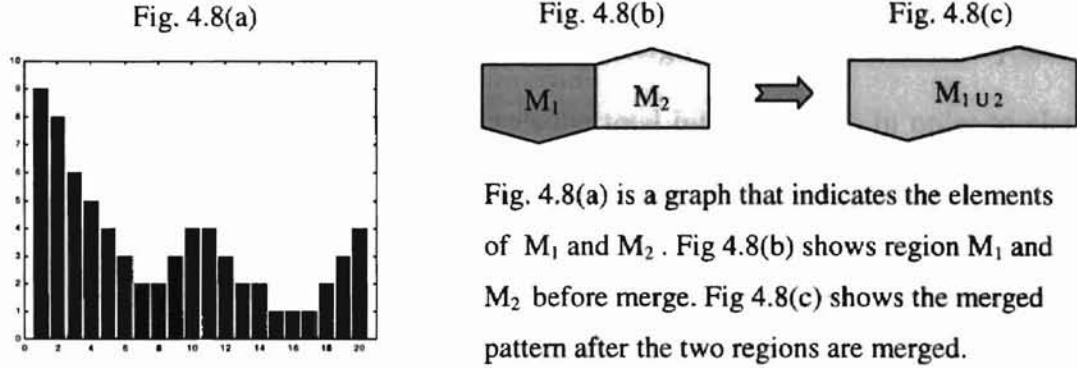
Fig. 4.8 An illustration of a merging process

In this example, $Var(M_1) = 5.82$ and $Var(M_2) = 1.34$. The weight is 10 pixels, thus the weighted variance (*SOV*) is given as $SOV_1 = 58.2$, and $SOV_2 = 13.4$. Using equation (12), the region energy, before and after merging, is given by

$$E_{before\ merge} = SOV_1 + SOV_2 + 2\lambda = 71.6 + 2\lambda, \tag{13}$$

$$E_{after\ merge} = SOV_{1\cup2} + \lambda = 95.7 + \lambda. \tag{14}$$

By solving the two equations, the scalability parameter λ is found. The energy gap ΔE, before and after the merge is defined by

$$\Delta E = E_{after\ merge} - E_{before\ merge}. \tag{15}$$

Without considering λ, ΔE has a positive number, *i.e.*,

$$E_{after\ merge} > E_{before\ merge}\ \text{or}\ E_{after\ merge} - E_{before\ merge} = \Delta E > 0. \tag{16}$$

Now, if we consider the scalability parameter λ, we accept the merge only if ΔE is negative, *i.e.*, a pair of regions can be merged only if $\Delta E < 0$. This means the total image energy must decrease during the merging process. According to this concept, λ is given by solving the equations (13) and (14). For $\Delta E < 0$,

$$95.7 + \lambda < 71.6 + 2\lambda,$$

$$\therefore 24.1 < \lambda.$$

Thus, the regions are merged by decreasing the total image energy only if $\lambda > 24.1$ in this example. When $\lambda = 24.1$, it is called the critical merging point and if λ is beyond the critical merging point, the merging decreases the total image energy. In order to clarify the energy level, several λ value are assigned to compute the region energy.

Table 4.2 The relationship of λ and ΔE

λ	$E_{before\ merge}$	$E_{after\ merge}$	ΔE
10	91.6	105.7	up
20	111.8	115.8	up
24.1	119.8	119.8	0
30	130.7	125.7	down

From this simple example, it is known that the scalability parameter (λ) works as a cost for merging. Additionally, λ controls the region scales, because in the equation, region size is considered. Therefore, λ can be also considered as a region scale parameter. When a small λ is applied, fine segmentations (large number of regions) are yielded. When a large λ is applied, coarse segmentations (few regions) are yielded. When the $\lambda = 0$, no regions can be merged, because without considering the λ, it always holds that

$$\Delta E = E_{after\ merge} - E_{before\ merge} > 0,$$

which does not meet the merging criterion $\Delta E < 0$.

This section studied the mechanism of the region merging process using our energy function. In the following subsection, we would like to show the advantage of the weighted-variance for the similarity criterion.

4.5.2 Similarity Measurement by the Variance versus Average of Region Graylevel

In the conventional region merging scheme, the average of the region graylevel was used for the similarity measurements. But, in the new merging scheme the region variance is used for the similarity criterion. There is a significant difference between the new and conventional schemes, because the region variance is more sensitive than the graylevel in comparison. This can be shown using an example. Shown below are the one dimensional regions (M_A) and (M_B). The M_B has modified the first and last terms of the sample region, M_A.

$$M_A = [9\ 8\ 6\ 5\ 4\ 3\ 2\ 2\ 3\ 4;\ 4\ 3\ 2\ 2\ 1\ 1\ 1\ 2\ 3\ 4] = [\,M_1\,,M_2\,].$$

$$M_B = [\underline{8}\ 8\ 6\ 5\ 4\ 3\ 2\ 2\ 3\,\textcircled{5}\,\textcircled{3}\ 3\ 2\ 2\ 1\ 1\ 1\ 2\ 3\,\textcircled{5}] = [\,M_3\,,M_4\,].$$

If we compare the average of the two regions, $Ave(M_1) = Ave(M_3)$ and $Ave(M_2) = Ave(M_4)$, but in the variance, $Var(M_1) \neq Var(M_3)$ and $Var(M_2) \neq Var(M_4)$. When we want to detect the difference between M_1 and M_3, or M_2 and M_4, how should we measure the differences? If we use the region average to measure the similarity, this criterion (region's average) can not detect the differences. Instead, if the region variance is used to measure region similarity, it can detect the transition of the region elements. During the merging process, it is possible that two regions' average are same, even if the large difference of the components (pixel values). Therefore, this causes merging error in the conventional merging scheme.

This subsection explained our new merging scheme and the similarity criterion using a simple example. In the following section, we expand this concept to the entire image. A hierarchical region clustering and hierarchical stepwise optimization clustering

algorithm are introduced. This algorithm merges the regions step by step according to the merging criterion, therefore this process forms a hierarchical merging structure. The following subsection shows how the hierarchical structure is effectively applied for the region merging scheme.

4.6 The Hierarchical Stepwise Merging Algorithm with the Variational Technique

In this algorithm, the hierarchical clustering starts from an over-segmented original watershed segmentation, assuming it has N regions. These regions are considered as *nodes*, and the number of the regions is sequentially reduced by merging. At each iteration, the cost for merging $C(R_i, R_j)$ is calculated for every pair of regions (R_i, R_j). Then the one pair of regions having the minimum merging cost is selected from entire regions and merged. This merging process is repeated sequentially until the desired number of regions are obtained.

One of the limitations of the hierarchical merging approach is the large computational cost for a large data set (large image size), because the merging cost for all of the possible pairs of regions have to be computed. If there are N regions, this computation can be $N \times (N-1)$. In our region merging case, however, only adjacent regions can be merged. This reduces the number of potential merging combinations per iteration to $N \times M$, where N is the number of regions, and M is the average number of neighbors. M is usually a small number, on average around $3 \leq M \leq 8$, and is quite independent of N (Beaulieu and Goldberg, 1989). Additionally, a merge affects only the surrounding regions, therefore only the adjacent regions need to be updated for the next evaluation. As a consequence, only a limited number of new segment pairs need to be

considered at each merging iteration. This is a major computational advantage obtained from the concept of the adjacent region clustering.

The algorithm of hierarchical merging with a sequential optimization process is now explained. The process starts with an initial watershed segmentation, $P_0 = \{R_1, R_2, R_3, \dots R_n\}$, and at each iteration, it merges pair of regions that have minimal merging cost. $C_{i,j}$ denotes the cost of the merging a pair of regions, i (R_i) and region j (R_j). The flow of the merging algorithm is as follow:

I – Initialization process:

1) $P_0 = \{R_1, R_2, R_3, \cdots ,R_n\}$ (initial segmentation derived from the watershed).

2) $\lambda = 0$, scalability parameter starts at 0, merging can start somewhere $\lambda > 0$.

3) Calculate SOV_k and NB_k (neighbors of region k) $\forall$ $R_k \in P_0$,

   where k is the image cardinality.

4) Calculate the merging cost $CS = \{ C_{i,j} | R_j \in NB_i \}$.

II – Merge most similar a pair of regions (the lowest cost region):

1) Find a pair of region that meet

$$C_{u,v} = \underset{C_{i,j} \in CS}{Minimum} (C_{i,j}) \text{ from the entire region.}$$

2) Region R_m is merged; $R_m = (R_u \cup R_v)$, which means replacement of the pair of regions to a newly merged region - m,

3) Calculate SOV_m of the merged region.

4) Update neighborhood information, $NB_m = (NB_u \cup NB_v) \cap \overline{\{R_u, R_v\}}$[1],

   which revises the information of the neighborhood

5) If no region can be merged at the given λ, increment it $\lambda = \lambda +1$.

---

[1] Taking the intersection with the complement corresponds to removing those elements from the set.

III – Stopping condition: Stop the merging algorithm if desired number of regions is obtained.

The initialization process, finding NB_k and computing SOV_k, are performed only once for a selected root level WS segmentation image. Thus, this algorithm is also designed to reduce the computational cost. In the initialization process, the computational cost is a function of the number of regions, the image size, and the number of neighbors per region. Instead, if the iteration steps are short, the computational cost is mainly a function of the number of regions R_n. The number of iterations depends on the number of initial regions, because each iteration reduces the number of segments by one.

Measurements of the Segmented Images

Once images have been segmented, the segmentation has to be evaluated to measure the quality. The quality can be measured by the total image energy according to (12). Now, assuming we want to compare two segmentation results from different techniques. If both images have the same cardinality (number of regions), we can simplify the equation (12) by only considering the variance-term. Then the segmentation quality can be evaluate by

$$\text{IQ}_{\text{image}} = \sum_i S_i \cdot Var(O_i) = \text{Image variance.} \tag{17}$$

The *IQ* represents image segmentation quality. This equation simply measures the smoothness at a given cardinality. Just like the image energy, at the given number of segments, the lower the *IQ* represents the better segmentation. When we compute image energy from different segmentation techniques, it is difficult to select a suitable λ. Therefore, if images have the same cardinality, we can compare the segmentation quality among different segmentation techniques by computing the image variances. This

segmentation evaluation technique is used when we compare the conventional and the new image segmentation results in Chapter-5.

Mean squared error (*MSE*) is often used to measure the differences of the processed image and the original image. The mean squared error is defined as

$$MSE = \{ \sum_x^N \sum_y^N \sqrt{[I_{org}(x, y) - I_{seg}(x, y)]^2} \} / N^2 , \qquad (18)$$

where I_{org} is the original image and I_{seg} is the segmented image. If the segmented image is an adequate representation of the original image, the *MSE* should yield a lower value.

In this thesis, we evaluated the segmentation results by measuring both image energy (or image variance) and the *MSE*. The lower these numbers, the better the segmentation results. All of the application results are shown in Chapter-5.

4.7 Application of the Variational Method on Synthetic Images

The previous section explained the segmentation evaluation techniques and the process of our image segmentation technique. This subsection explains the relationship between the segmentation result and the image energy using simple synthetic images.

A synthetic test image-A, which is 8x8 square, is shown in Fig.4.9. There are five regions, R_1 - R_5, and each region has a different graylevel. The initial weighted variance of each region and the region number is shown in the following table.

Fig.4.9(a)   Fig.4.9(b)

Fig.4.9 An original synthetic test image and the initial partitions
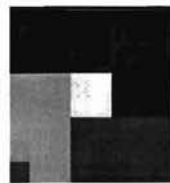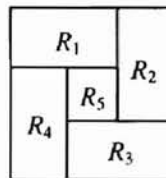
Table 4.3 Initial variance of the test image

Region	Initial *SOV*
R_1	296.1
R_2	206.7
R_3	139.0
R_4	4119.6
R_5	57.3

In this experiment, we merged the original image until two regions were formed from the original five. There are a total of thirteen possible patterns that can be formed for the two region segmentations.

These patterns are shown in the Fig.4.10 $P_2(1)$-$P_2(13)$. The segmentation result from the variational technique is shown in Fig.4.10 $P_2(13)$vt. The number of possible pattern is much less than $_5C_2$ (combination of five from two), because regions will merge with only those connected regions.

Fig.4.10 Thirteen possible segmentation patterns
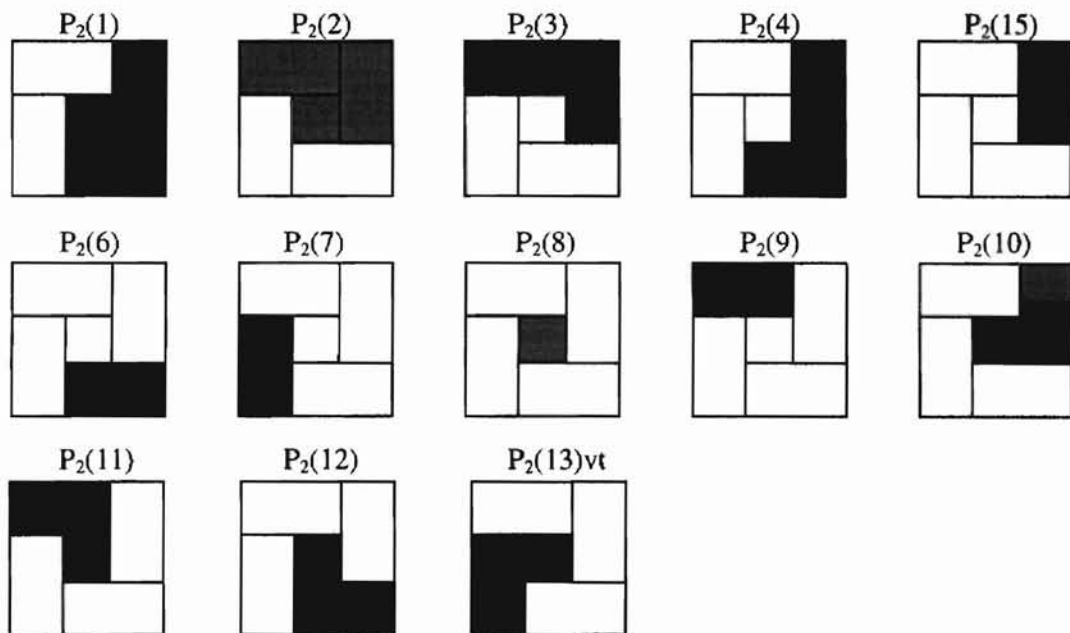
All of the thirteen patterns are computed using the image energies and the *MSE*. The results are summarized in the following Table 4.4. The pattern numbers are shown from $P_2(1)$ through $P_2(13)$vt, and the $P_2(13)$vt is the segmentation result from our variational technique. The energy is calculated according to the equation (12), and the mean squared error is computed from equation (18).

Table 4.4 Calculated MSE and the energy for the thirteen patterns

Pattern	$P_2(1)$	$P_2(2)$	$P_2(3)$	$P_2(4)$	$P_2(5)$	$P_2(6)$	$P_2(7)$
MSE	109	89.4	80.5	83.7	74.4	109	79.6
$E_{(x10^3)}$	322	206	89	304	282	317	189
Pattern	$P_2(8)$	$P_2(9)$	$P_2(10)$	$P_2(11)$	$P_2(12)$	$P_2(13)$vt	
MSE	114	91.2	116	102	101	53.8	
$E_{(x10^3)}$	233	178	322	287	284	82	

As shown in above table, both the segmentation energy and the *MSE*, which from the variational technique indicated lowest value. In other words, our variational algorithm found the best segmentation in the two region segments. Next we want to show the segmentation results that form four regions and then three regions and consider the path of the region merging.

Merging Path and Local Minimum Image Energy

In the previous section, we studied the segmentation energy of only two regions. Here, we want to examine the image energy for three and four region segmentations to show the merging path and the energy level. We want to show that the merging technique consistently produces the lowest image segmentation for each number of segments.

Energy Computation for Four Regions

There are a total of eight segmentation patterns that can be formed from the given image pattern. We have computed the energy of all the possible segmentation patterns, and the results are shown in Table 4.5. In the table, $P_4(8)$vt is the segmentation pattern from our variational algorithm. The error and energy are the lowest among all of the possible segmentations. Next, we repeated the same computations for three regions.

69

Table 4.5 Calculated MSE and the energy for the possible patterns for four segmentation

Pattern	$P_4(1)$	$P_4(2)$	$P_4(3)$	$P_4(4)$	$P_4(5)$	$P_4(6)$	$P_4(7)$	$P_4(8)$vt
MSE	49.8	41.5	32.1	26.5	35.1	32.9	88.3	15.0
$E_{(x10^3)}$	170.1	114.7	61.2	17.9	25.4	44.0	213.2	16.3

Energy Computation for Three Regions

In order to examine the energy level and the errors for three regions, we computed all possible segmentation patterns which form three regions. There are a total of 20 possible patterns. The segmentation energy and error (*MSE*) are summarized in the following table. Again in this experiment, our variational merging algorithm found the lowest energy segmentation, which is indicated as $P_3(20)$vt in Table 4.6.

Table 4.6 Calculated MSE and the energy for the possible patterns for three segments

Pattern	$P_3(1)$	$P_3(2)$	$P_3(3)$	$P_3(4)$	$P_3(5)$	$P_3(6)$	$P_3(7)$
MSE	51.6	50.1	44.4	74.8	48.6	65.2	88.3
$E_{(x10^3)}$	116.4	113.6	76.3	284.3	70.9	121.3	211.9
Pattern	$P_3(8)$	$P_3(9)$	$P_3(10)$	$P_3(11)$	$P_3(12)$	$P_3(13)$	$P_3(14)$
MSE	50.4	99.1	79.9	43.5	72.6	77.7	107.1
$E_{(x10^3)}$	57.2	233.7	153.9	36.8	269.5	209.4	323.0
Pattern	$P_3(15)$	$P_3(16)$	$P_3(17)$	$P_3(18)$	$P_3(19)$	$P_3(20)$vt	
MSE	76.0	48.6	65.1	66.6	114.9	34.5	
$E_{(x10^3)}$	190.7	74.3	184.3	173.6	227.8	29.4	

Through these experiments, we computed all possible segmentations for two, three, and four regions. The segmentation results from our algorithm using variational technique yielded the lowest energy and the lowest error of any segmentation pattern for each number of segments. Another interesting point is that this algorithm found the path of the lowest energy in each segmentation. This is a meaningful result.

Fig.4.11 The region merging results from variational technique on a synthetic image-A
(a) 5 regions   (b) 4 regions   (c) 3 regions   (d) 2 regions

The segmented image, Fig.4.11(d), is the result of our two region segmentation from our region merging technique. As we explained earlier, the segmentation pattern has the lowest energy and *MSE* of any segmentation pattern(with two regions). Just as for the two region segmentation, all of the paths (four and three regions) also had the lowest energy for each number of segments. The merging path is shown in Fig4.11.

Fig.4.12 The region merging results from variational technique on a synthetic image-B
(a)11 regions   (b) 9 regions   (c) 7 regions   (d) 5 regions
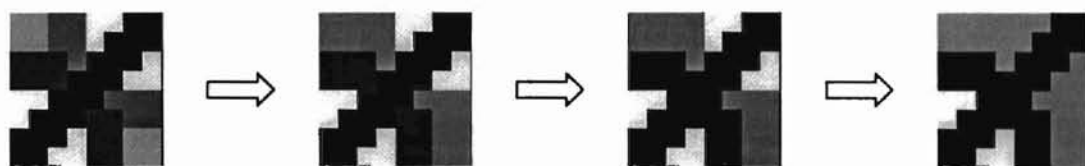
We also examined the same experiment on the second synthetic image, Fig.4.12. The results showed the merging path from the original partition, Fig.4.12(a) to five regions (three graylevel classification), Fig.4.12(d). From the variational technique, the lowest energy segmentation patterns were found for each number of regions.

In this section, we examined our new region merging technique showing the merging results on simple synthetic images. The results from the synthetic images show adequate segmentation results. The results from the variational technique yielded the lowest *MSE* and the lowest image energy in each segmentation. These are encouraging results and it increase our confidence in applying this merging technique to more complex images. In the following chapter, we will apply this merging technique to more

realistic images – soil moisture images. The segmentation results from the conventional segmentation technique and our new merging technique are fully compared.

4.8 Summary

This chapter explained our solution to two issues of watershed segmentation – large computational cost and over-segmentation. To reduce the computational cost, we applied the concept of the image pyramid. Gauch and Pizer introduced the multi-resolution watershed technique(Gauch and Pizer, 1993), but in our multi-resolution watershed pyramid WS is applied at a root level and the WS boundaries are propagated to the original image size. This approach can reduce the computational cost significantly, because the WS is applied to each intermediate layer *only* on the boundaries.

For the application of the WS algorithm to the soil moisture imagery, we introduced the new merging algorithm by applying the concept of a variational model. We formulated an energy function, then progressed the merging according to the energy level. The original energy function can be seen in the Morel's study. But in our merging scheme, the region scale parameter, λ is increased gradually until desired number of regions is yielded. We applied this process, because it is a possible way to find a local minimum energy in the cardinality. From our synthetic image examples, this merging technique adequately found local minimum energy in each segment. The segmentation results also showed the lowest energy and the lowest MSE in each segmentation result.

Using the concept of image energy with the energy equation, we obtained a new image segmentation evaluation criterion. In the following chapter, we will apply the new merging algorithm to the actual soil moisture images. The segmentation results are

measured by both *MSE* and image energy (image variance), and these results are evaluated by comparing the conventional segmentation with the new segmentation method.

Chapter 5. Results and Conclusions

5.1   Introduction

In the previous chapter, we introduced a new region merging technique and a segmentation evaluation criteria using a variational technique. This chapter demonstrates the region merging techniques and summarizes the segmentation results. Image segmentations are implemented by two types of region merging techniques and the segmentation results are compared. The segmented images are measured by two metrics, the image energy and mean squared error (*MSE*) as explained in Chapter-4. The smaller values represent the better segmentation results in both measurements.

Another improvement on the conventional watershed segmentation is the application of the multi-resolution watershed pyramid. Using the multi-resolution watershed (WS), the computational time is significantly reduced. The multi-resolution pyramid creates a scale-space and the WS is applied at a selected root level, which is a coarse representation of the original image. Once the WS is applied at a root level, the WS boundaries are propagated to the original image size. During the propagation process, the WS is applied only on the boundaries in each layer. Therefore a significant reduction in computational cost is expected. We compared the computational cost with and without applying the multi-resolution pyramid on the soil moisture images, and the results are shown in this chapter. Section 5.3 concludes and discusses all of the research findings and contributions in this thesis. Finally, section 5.4 mentions some proposals for future work.

5.2   Image Segmentation Results

The objective in this section is to compare and contrast segmentation results from the new and conventional region merging approaches. In this experiment, a total of five images are used. For the first two, we selected relatively simple images, which have a clear target object and are well contrasted. These types of images are often used for the evaluation of image segmentation techniques.

For the soil moisture image segmentation, we chose three sub-regions from the original satellite imagery. Segmentation conditions are summarized in Table 5.1 and the segmentation results are examined in the following section.

Table 5.1 Application of Image Segmentation

Category :	Image name:	Image size:	Root level :	Merging method :	Figure number
Test Image	Swan	256	1(128)	Recursive Threshold	Fig 5.1(a)
	Swan	256	1(128)	Variational Technique	Fig 5.1(b)
	Leaf	256	2(64)	Recursive Threshold	Fig 5.2(b)
	Leaf	256	2(64)	Variational Technique	Fig 5.2(c)
Soil Moisture	SMr13c07(River)	512	1(256)	Recursive Threshold	Fig 5.3(a)
	SMr13c07(River)	512	1(256)	Variational Technique	Fig 5.3(b)
	SMr04c04(Field)	512	1(256)	Recursive Threshold	Fig 5.4(a)
	SMr04c04(Field)	512	1(256)	Variational Technique	Fig 5.4(b)
	SMr11c10(Lake)	512	2(128)	Recursive Threshold	Fig 5.5(a)
	SMr11c10(Lake)	512	2(128)	Variational Technique	Fig 5.5(b)

5.2.1   Application of Region Merging to Test Images

The purpose of the test images is to show the efficiency of the region merging methods before applying them to complex soil moisture images. If the segmentation

technique shows valid segmentation results from relatively simple images, the segmentation results from the soil moisture images will be more reliable. A swan image and a leaf image are chosen for the test images. Each of these images is well contrasted and has a clearly identified target object. In order to compare the region merging schemes, the segmentation results are measured by both mean-squared-error and the image variance. The segmentation results are explained below.

Segmentation Results from the Swan Image

The segmentation results from the swan image are shown in Fig.5.1(a) and Fig.5.1(b). Fig.5.1(a) shows the segmentation results from the conventional merging scheme using recursive thresholding. Fig. 5.1(b) shows the segmentation results from the new merging scheme using the variational technique. The top-left image in the figure is over-segmented at the root level WS mosaic image (region merging starts from this image) and the rest of the images show the region merged results. In the figures, R stands for the number of regions in the image, image variance is denoted as V and mean-squared-error of the image is denoted as MSE. Starting from the over-segmented original WS mosaic image, we attempt to merge them to a desired number of regions. In this experiment, the number of regions is selected from 300 to three regions. Comparing Fig.5.1(a) and 5.1(b), visually there are few differences. But each image from the new merging scheme, in Fig.5.1(b), has superior variance and MSE to those of the corresponding conventional segmentations, in Fig.5.1(a). In the next test image, we corrupt an original image by salt-and-pepper noise, then examine the same sequence for the Leaf image.

Segmentation Results from the Leaf Image

In this experiment, we wanted to demonstrate how noise affects the WS segmentation and the region merging process. A corrupted image is made by adding 30 percent salt-and-pepper noise to the original image. During the multi-resolution WS segmentation, each layer of the image is sequentially open-close filtered, then sub-sampled. The original image, noisy image, and filtered images are shown in the Fig.5.2(a). From the images, the filtering effects are easily observed. In root level three, the noise is eliminated by the sequential filtering, yet the original leaf still can be recognized. This root level is selected for further watershed segmentation, and the region merging results are shown in Fig.5.2(b) and 5.2(c).

Starting from the over-segmented watershed mosaic image (root image size = 64), region merging progresses until the leaf is segmented from the background. In this experiment, the number of regions is selected from 150 to two regions. In our region merging algorithm, the regions are merged one by one in each merging iteration. The region merging results from the conventional scheme are shown in Fig.5.2(b), and the results from our variational technique are shown in Fig.5.2(c). Both schemes clearly segment the leaf image from the original over-segmented mosaic image. Visually, a small merging mistake can be identified from the result of the conventional merging scheme. In order to clarify the difference, measuring the image variance and *MSE* are helpful. Comparing both the image variance and *MSE*, we can recognize that the segmentation results from the new merging scheme are a better representation of original image.

5.2.2 Soil Moisture Image Segmentation

For the soil moisture segmentation, we selected three regions from the original satellite sensed region. The first image was chosen from the south of Oklahoma, on the border of Oklahoma and Texas, which includes the Red River. This image includes bodies of water, and would show strong soil moisture contrast when they are segmented.

The second image was selected from the region that does not contain large bodies of water, and is acquired from near the northwest corner of the whole image. This region was selected because it had relatively strong contrast of soil moisture distribution than other SM images. The third region was selected from the region that included the Waurika Lake and includes large bodies of water.

The selected soil moisture image is about 12km x 12 km in area, which makes a 512x512 pixel image. The root level two (root image size = 256) was used for both Red River and Field image and root level three (root image size = 128) was used for the Waurika Lake image. These root levels are selected because significant features are lost above the root level by the open-close filtering and sub-sampling.

Soil Moisture Segmentation on SMr13c07 Image: Red River region

The segmentation results from both the conventional region merging and the new merging techniques are shown in Fig.5.3(a) and 5.3(b) respectively. The original over-segmented WS mosaic image is displayed in the top-left corner of the figure. Starting from the over-segmented image, the merging results from 200 regions to 15 regions are displayed. The image variance and *MSE* are measured for every image and they are indicated as individual image subtitles.

By comparing both segmentation results, it is easy to recognize the qualitative differences. The segmentation results from the conventional merging scheme merged the regions too rapidly. The river and slight soil moisture distribution on the fields were also merged in the early merging stages. Nevertheless, the conventional merging scheme leaves small regions as spots until the end of the merging.

In the segmentation results from the variational technique, regions are merged gradually and small regions are merged in the early merging stages. This demonstrates the advantage of being able to control the region scalability in the variational merging technique. The segmentation quality is easily known by comparing the image variance and *MSE*. Both the image variance and the *MSE* from the new region merging results show superior numbers compared to those of the conventional scheme.

The edge maps (the boundaries of the WS segmentation) are shown in Fig.5.6(a). The original SM image, the SM image at the root level, the over-segmented WS mosaic image, the merged image (at the number of regions is 30), and the edge map are provided. From the figure, it may be observed that the WS mosaic image is a reasonable representation of the original SM image at the selected root level. The edge map shows closed and thin WS boundaries of the merged image. The number of regions is selected arbitrarily by the author. This selection is used to exhibit the WS boundaries; the edge map can be for any number of regions.

Soil Moisture Segmentation on SMr04c04 Image: Field region

Image segmentation results from the SMr04c04, Field regions are shown in Fig. 5.4(a) and 5.4(b). The region merging results from the conventional technique are shown in Fig.5.4(a) and the results from the new merging technique are shown in Fig.5.4(b).

Compared to the Red River image, this field image tends to be more uniform in soil moisture distribution, because of the absence of bodies of water. Using the conventional region merging scheme, the region merging results yielded a poor representation of the original soil moisture image. Similar regions are rapidly merged in the early stages, and the segmented patterns are far from the original SM distribution. Instead, each merging result from the variational technique showed a more reliable soil moisture pattern than those of the conventional scheme, as measured by the image variance and *MSE*. Both numbers for each segmentation using the new merging scheme were better than those of the corresponding conventional segmentation.

The corresponding edge maps are shown in Fig.5.6(b). The original SM image, the SM Image at the root level, the over-segmented WS mosaic image, the merged image (at number of regions is 30), and the edge map are exhibited. From the figure, it is seen that the WS mosaic image nicely represents the original SM image. The edge map also shows closed and thin WS boundaries of the merged image.

Soil Moisture Segmentation on SMr11c10 Image: Lake region

The third soil moisture region includes large bodies of water, the Waurika Lake image. In the previous two regions, the root level two was used. Here we selected root level three. The merging results from the conventional merging scheme are shown in the Fig.5.5(a), and those results from the new merging scheme are shown in the Fig.5.5(b). As with the previous segmentation results, the new merging scheme creates a more reliable soil moisture distribution than the conventional merging scheme in each segmentation, because of the smaller *MSE* and variance. The results show that the conventional scheme merges similar graylevel regions too rapidly and small details

80

remain until a later merging stage. This tendency is quite common in all of the results of the conventional merging scheme. Both image variance and *MSE* from the new technique reveal much improved results over those of the conventional scheme. The new merging technique also showed the excellent controllability of region scalability in this experiment.

The edge maps are displayed in Fig.5.6(c). Comparing the previous two root levels, this root level image is a more coarse representation of the original SM image, because of the higher root level selection. Nevertheless, the region merging results are a good representation of the original WS mosaic image. The edge map displays the closed and thin boundaries of the segmentation.

5.3   Conclusion and Discussion

The Computational Cost of the Watershed Segmentation

Through this thesis, we have sought possible solutions to the two weaknesses of the watershed segmentation, which are the large computational cost and over-segmentation. Applying the concept of the image pyramid, substantial computational costs have been reduced. Without using the image pyramid (fixed-resolution watershed), on the average it takes about 19 minutes to process a watershed segmentation on a 512x512 image in the C program by a Unix Workstation. Instead, by applying multi-resolution watershed at root level two (image size = 256), on the average it required about 1.6 minutes, and at root level three (image size = 128) only about 29 seconds were required. The results of the computational cost from three SM images are summarized in the Table 5.2. This algorithm was also translated to Matlab codes, and examined for

performance. The Matlab programs run slower than C program, but the computational costs were reduced by similar proportions in the multi-resolution watershed.

Table 5.2 The computation costs of the fixed WS and the multi-resolution WS

Image (size) :	Fixed-Resolution : (512x512)	Multi-Resolution Root =1(256x256)	Multi-Resolution Root =2(128x128)
SMr13c07	21.95 min	1.93 min	31 sec
SMr04c04	18.53 min	1.52 min	27 sec
SMr11c10	16.72 min	1.30 min	28 sec
Average	19.07 min	1.60 min	29 sec

The reduction of computational costs directly relates to the selection of the root level. The higher root level selection, the less computation cost. But selection of a high root level sacrifices the resolution of the image. In the experiments of soil moisture image segmentation, we used root level one for the Red River and the field image, and root level two was used for the Waurika Lake image. Comparing the original SM image and the root level image, in Fig.5.6, the difference is recognized. As a consequence, the selection of the root level will depend on how much detail is demanded.

Region Merging by Variational Model and the Evaluation Criteria

For a possible better solution to the over-segmentation issue, we introduced the new region merging technique - an application of the variational model. The major difference in the proposed method from the conventional approach is that the region similarity is measured by the weighted-variance, instead of the region graylevel. An energy equation is formed as (12), and in our merging technique the λ is monotonically increased till desired number of segmentation is yielded. We applied this scheme because, it is a possible way to find a local minimum image energy in the cardinarity.

Experimental results by the new and the conventional region merging were fully

demonstrated in section 5.2. The segmentation results are measured and also visually

evaluated. Both image variance and *MSE* from the new merging method were superior to

those from the conventional merging technique. From the visual comparison, the

advantage of the new merging scheme is easily observed. Significant differences were

observed from the segmentation results between the new and the conventional method on

soil moisture images. These results tell us that the conventional merging scheme could be

applicable only to those simple images, but not for more complex images, such as soil

moisture images. Because the soil moisture images have more uniform distribution in the

image intensity, the image segmentation requires a more critical criterion. Additionally,

the new region merging technique showed superior region scale controllability in the

merging results (uniform region size), because our energy equation considers the region

size during the merging process. This is another significant difference from the

conventional merging technique. Consequently, the proposed new region merging

scheme showed excellent segmentation results in this experiment.

Discussion

Using the variational technique and an image energy function, we attempted to

minimize the image energy, and eventually segment the image. If we look at the merging

scheme from the concept of image energy, this process is identical to finding a local

minimum of the image energy. Because the energy equation is designed to find a path

toward lower energy. It is like dropping a ball from the top of a hill in a given relief

(solution space), as the ball would reach a lower point (local minimum), but we do not

have any guarantee that it is the lowest point (global minimum) of the entire surface. In order to find the global minimum, the ball would have to be able to climb up slopes or hills. In our algorithm, the ball is allowed to go only downward; climbing is not allowed. A hill-climbing algorithm is possible, but practically it requires extensive computational costs, because it has to search every possible direction. Also it does not know where (what energy value) is the global minima. Therefore, it does not find a stopping point until every possible trial has been examined. Our algorithm is constantly searching to reduce the energy and eventually reach a local minimum.

There is one more constraint in our region merging algorithm, the regions are constantly merged but not allowed to split up. This constraint could interfere with finding the global minimum. But, again if we implement the algorithm in a practical image size, the split and merge operation requires an extremely large computational cost.

5.4   Future Work

In this section, we would like to propose several research topics for the further study. First, we did not consider the concept of image energy during the process of the WS segmentation. The image energy is considered and minimized from a given WS segmentation result. So, we have a missing link between original images and WS segmented images. We think that the concept of image energy can be applicable during the WS segmentation process. One idea is to form the WS segmentation using a variational technique to minimize image energy.

Finding the global minimum of image energy is an additional area of future work. One solution to finding the global minimum is the application of an annealing technique.

This technique could find the lowest energy from the *all* possible segmentations. Therefore, it requires a very large computational cost (nearly infinity) to compute the best answer for the practical image size. Without using computer simulation, mathematically it may be possible to create an algorithm to reach the global minimum.

Through this thesis, we have applied the variational technique for region merging process. Compared to the conventional merging technique, this technique is well motivated and significantly improved the segmentation results. But it is just one application of the technique, and we hope our results encourage for the further application of this technique. Fortunately, the variational technique is flexible and it is widely applicable. As the technique yielded excellent results in our application, we believe this technique offers a better solution to various field of image processing.

Fig.5.1(a) Segmentation results from recursive thresholding on Swan image

Swan Image Root Size = 128

Original Image	$R=300$, $V=103.7$, $MSE=23.5$	$R=100$, $V=107.9$, $MSE=26.5$

$R=80$, $V=110.1$, $MSE=27.3$	$R=40$, $V=121.6$, $MSE=30.8$	$R=20$, $V=153.2$, $MSE=40.3$

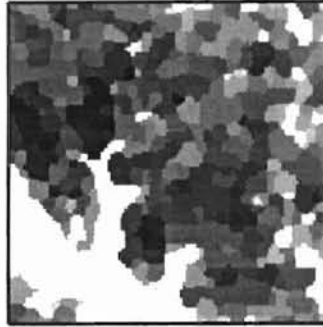| $R=10$, $V=229.6$, $MSE=58.1$	$R=5$, $V=303.4$, $MSE=74.8$	$R=3$, $V=319.1$, $MSE=76.1$

(R = the number of regions, V= the image variance, MSE = the mean squared error)

Fig.5.1(b) Segmentation results from variational technique on Swan image

Original Image

R=300, V=91.5, MSE=22.0

R=100, V=93.9, MSE=23.8

R=80, V=98.3, MSE=24.5

R=40, V=102.9, MSE=27.2

R=20, V=118.7, MSE=31.8

R=10, V=151.5, MSE=40.5

R=5, V=184.3, MSE=48.7
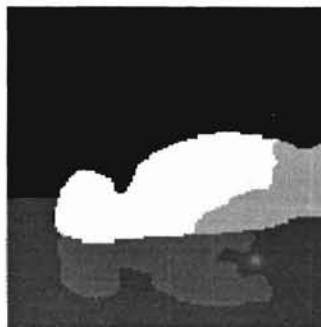
R=3, V=304.4, MSE=66.1

(R = the number of regions, V= the image variance, MSE = the mean squared error)

Fig.5.2(a) Noisy Leaf image and open-close filtered images

Original Image
Size=256

Noisy Original Image
Size=256
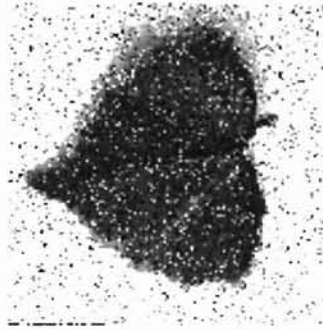
Filtered Image
Size=256, Root Level=0

Filtered Image
Size=128, Root Level=1

Filtered Image
Size=64, Root Level=2

Fig.5.2(b) Segmentation results from recursive thresholding on Leaf image

Root Size = 64
Original WS Mosaic Image   *R*=150, *V*=290.6, *MSE*=34.8   *R*=100, *V*=289.6, *MSE*=34.9
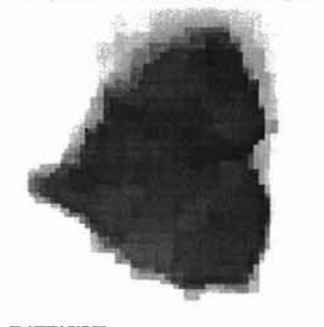
R=80, *V*=289.6, *MSE*=35.0   *R*=40, *V*=290.8, *MSE*=35.5   *R*=20, *V*=308.4, *MSE*=38.0
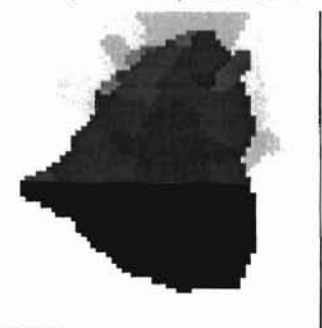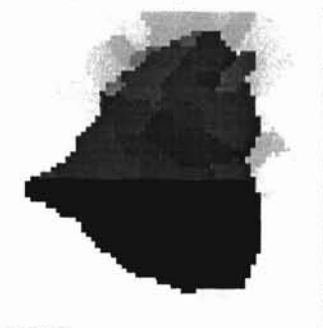
R=10, *V*=365.5, *MSE*=46.2   *R*=5, *V*=429.6, *MSE*=57.1   *R*=2, *V*=459.5, *MSE*=58.1

(*R* = the number of regions, *V*= the image variance, *MSE* = the mean squared error)

Fig.5.2(c) Segmentation results from variational technique on Leaf image

Original WS Mosaic Image	$R=150$, $V=91.5$, $MSE=33.2$	$R=100$, $V=93.9$, $MSE=33.4$

$R=80$, $V=98.3$, $MSE=33.5$	$R=40$, $V=102.9$, $MSE=33.9$	$R=20$, $V=118.7$, $MSE=35.5$

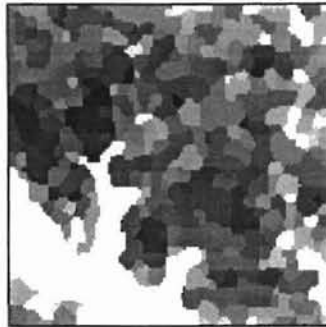| $R=10$, $V=151.5$, $MSE=40.3$	$R=5$, $V=184.3$, $MSE=48.2$	$R=2$, $V=304.4$, $MSE=57.9$
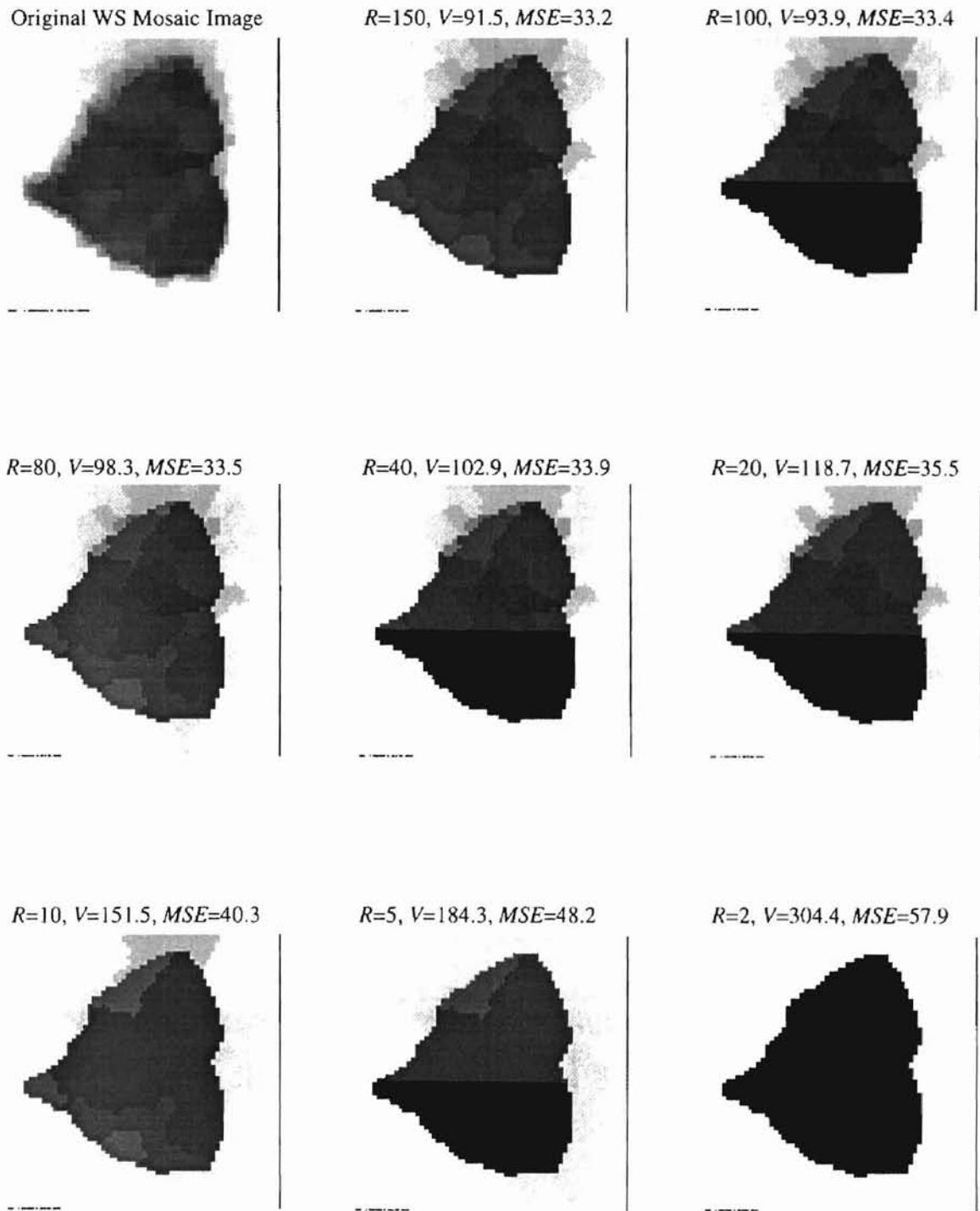
(R = the number of regions, V= the image variance, MSE = the mean squared error)

Fig.5.3(a) SM segmentation results from recursive threshold on SMr13c07 image
(Red River Image)

Root Size = 256 : R=2151
Original WS Mosaic Image
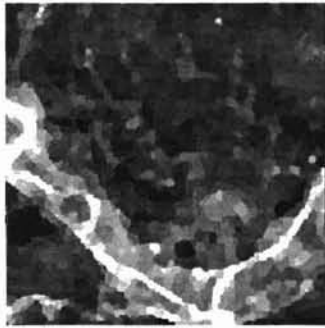
R=200, V=287.2, MSE=64.7
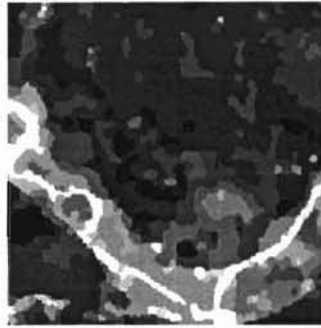
R=100, V=375.1, MSE=89.3
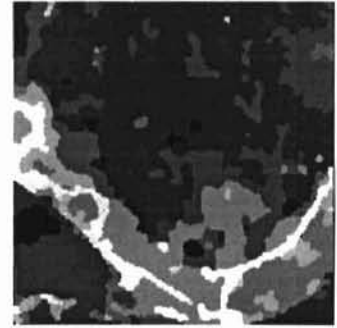
R=80, V=396.1, MSE = 92.3
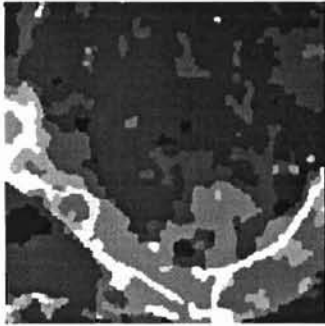
R=60, V=550.2, MSE = 118.8
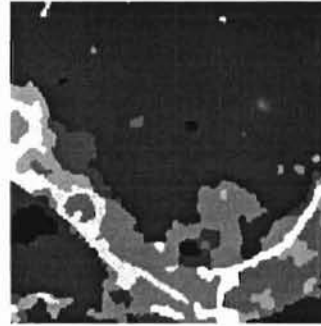
R=50, V=557.8, MSE =119.7
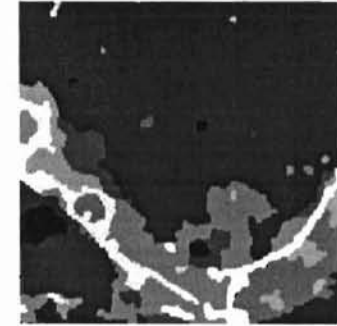
R=40, V=622.3, MSE =132.3
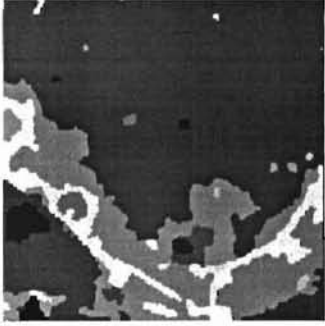
R=35, V=644.2, MSE =135.6
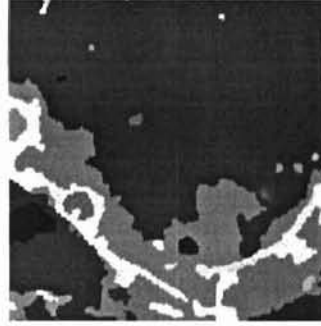
R=30, V=660.9, MSE =137.0
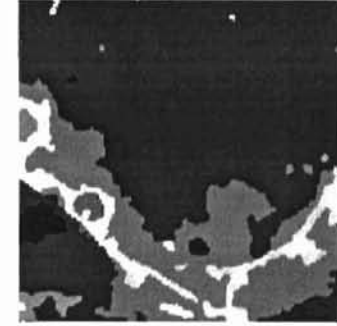
R=25, V=684.7, MSE =137.7
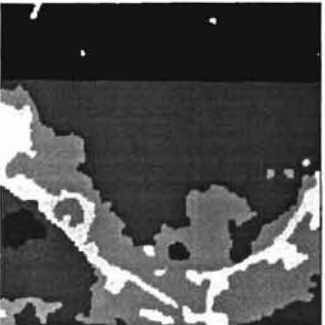
R=20, V=994.4, MSE =169.3
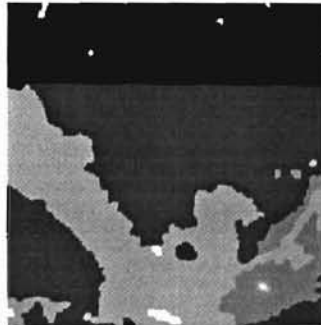
R=15, V=1037, MSE =170.6
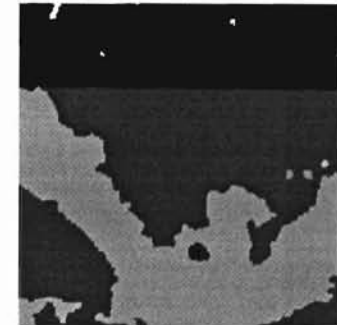
(R = the number of regions, V= the image variance, MSE = the mean squared error)

Fig.5.3(b) SM segmentation results from variational technique on SMr13c07 image

Root Size = 256 : R=2151
Original WS Mosaic Image
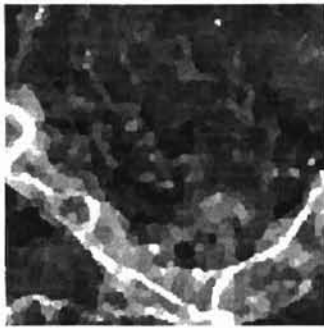
R=200, V=264.5, MSE=51.6
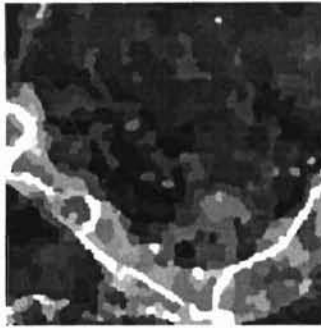
R=100, V=264.5, MSE=51.6
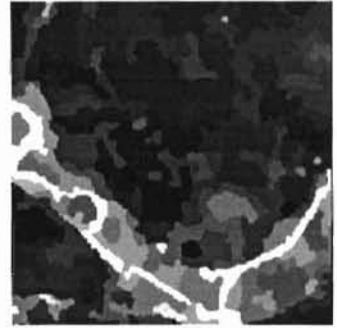
R=80, V= 291.1, MSE=58.1
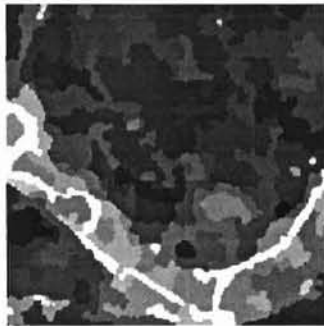
R=60, V=321.8, MSE=64.0
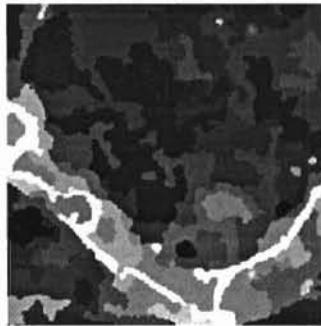
R=50, V=347.4, MSE=69.1
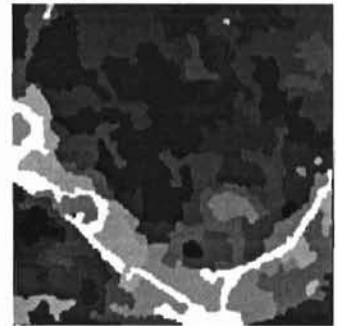
R=40, V=378.1, MSE=75.3
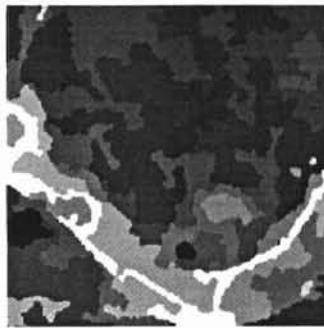
R=35, V=400.8, MSE=79.7
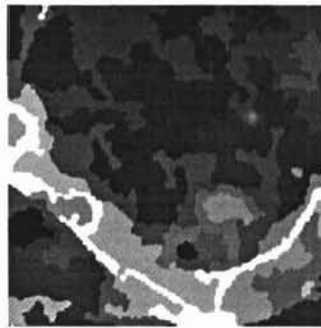
R=30, V=428.5, MSE=84.1
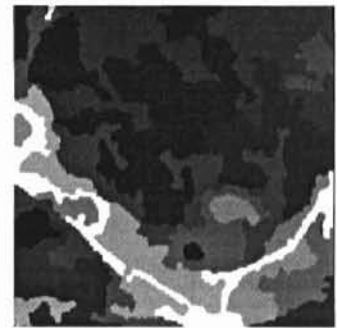
R=25, V=459.1, MSE=88.5
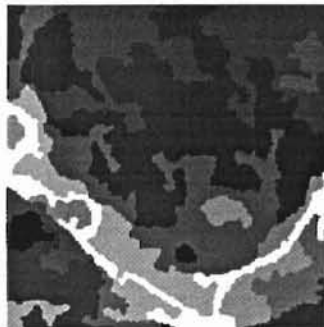
R=20, V=515.7, MSE=97.7
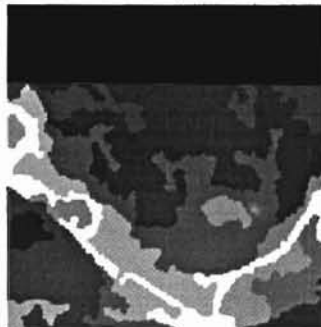
R=15, V=608.3, MSE=110.8
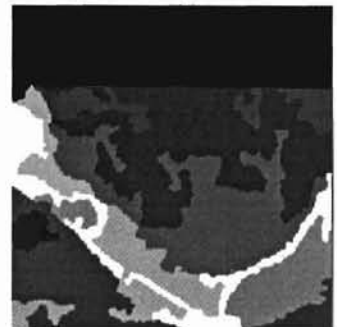
(R = the number of regions, V= the image variance, MSE = the mean squared error)

Fig.5.4(a) SM segmentation results from recursive threshold on SMr04c04 image
(Field Region)

Root Size = 256 : *R*=2077
Original WS Mosaic Image
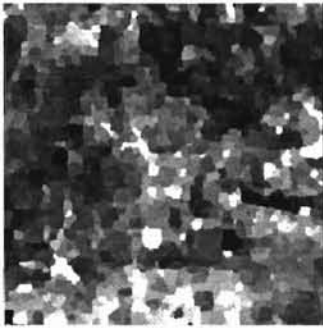
R=200, *V*=475.5, *MSE*=94.4
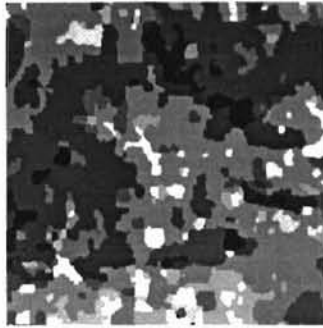
R=100, *V*=664.7, *MSE*=123.3
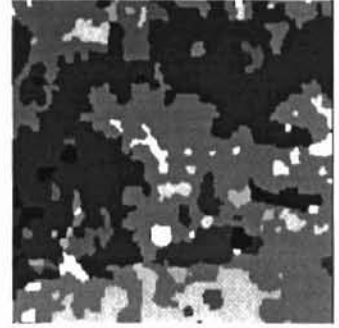
R=80, *V*=782.9, *MSE*=142.3
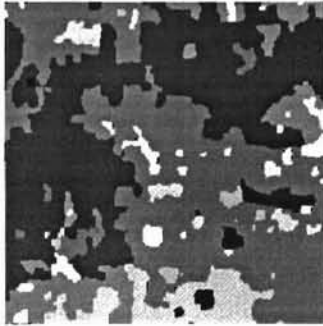
R=60, *V*=1073, *MSE*=170.7
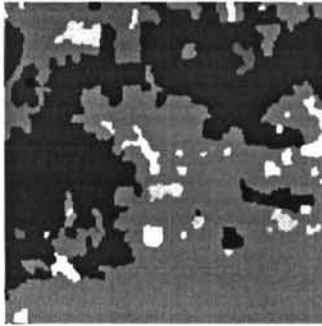
R=50, *V*=1357, *MSE*=205.6
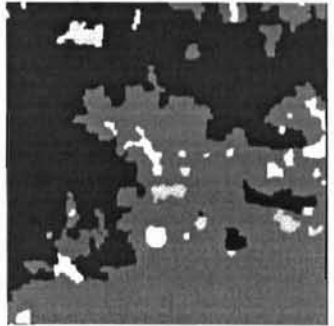
R=40, *V*=2350, *MSE*=332.7
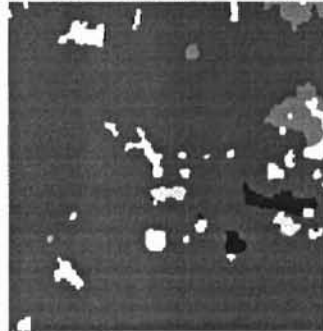
R=35, *V*=2427, *MSE*=335.9
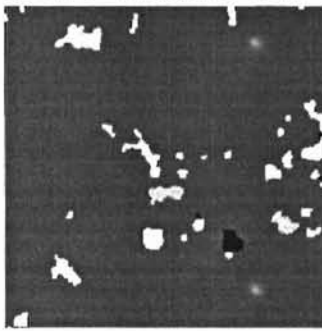
R=30, *V*=2598, *MSE*=336.5

R=25, *V*=2617, *MSE*=339.9
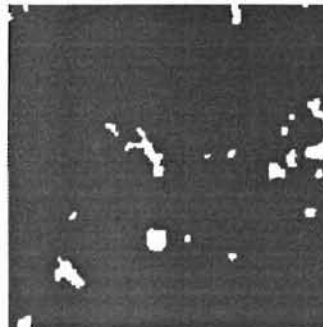
R=20, *V*=2691, *MSE*=345.9
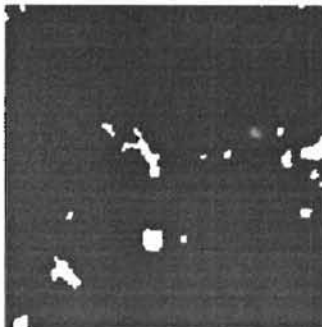
R=15, *V*=2712, *MSE*=352.5

(*R* = the number of regions, *V*= the image variance, *MSE* = the mean squared error)

Fig.5.4(b) SM segmentation results from variational technique on SMr04c04 image
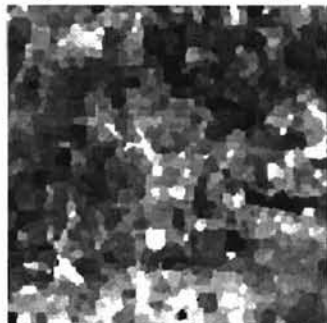
Root Size = 256 : R=2077
Original WS Mosaic Image   R=200, V=350.6, MSE=74.3   R=100, V=474.7, MSE=93.48
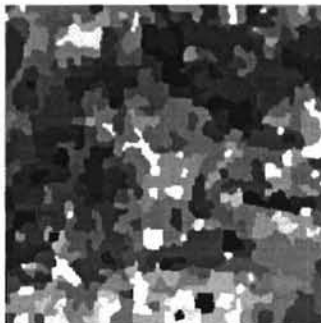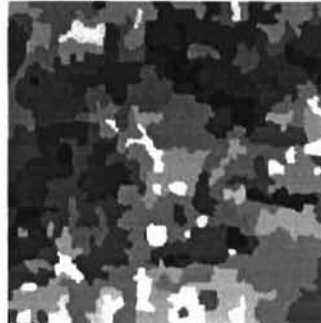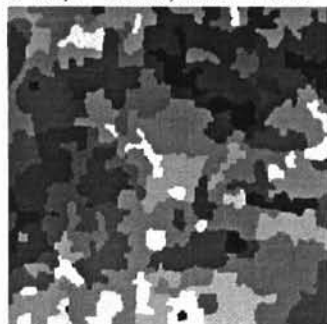
R=80, V=526.5, MSE=101.1   R=60, V=600.4, MSE=111.5   R=50, V=653.1, MSE=119.5
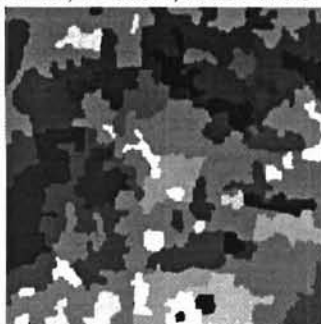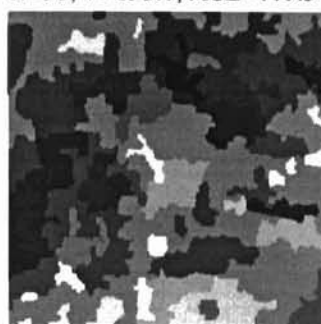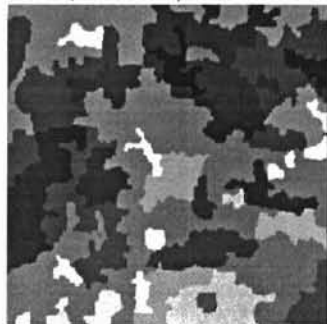
R=40, V=729.2, MSE=128.3   R=35, V=774.4, MSE=134.7   R=30, V=836.7, MSE=141.7
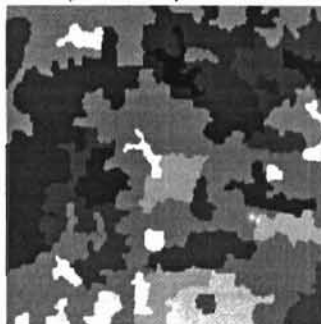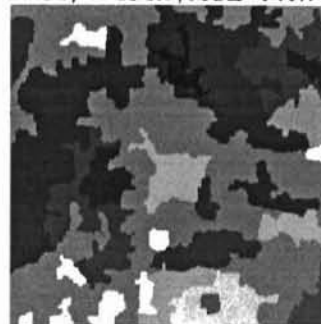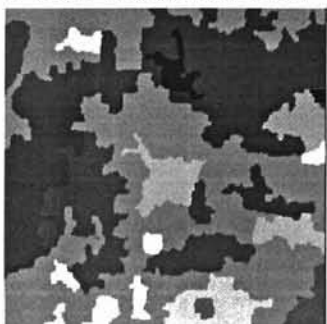
R=25, V=903.0, MSE=149.7   R=20, V=985.2, MSE=157.6   R=15, V=1108, MSE=174.7
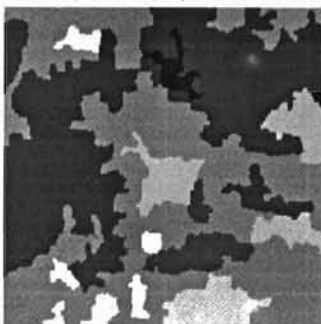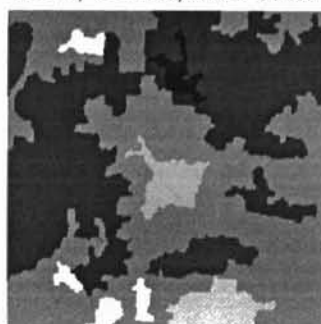
(R = the number of regions, V = the image variance, MSE = the mean squared error)

Fig.5.5(a) SM segmentation results from recursive threshold on SMr11c10 image
(Waurika Lake)

Root Size = 128 : *R*=553
Original WS Mosaic Image
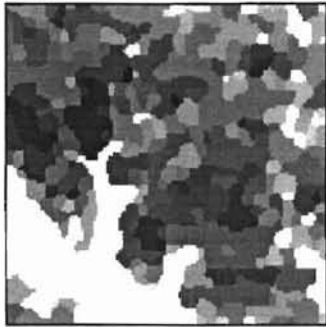
R=200, *V*=287.3, *MSE*=50.5

R=100, *V*=383.8, *MSE*=63.6
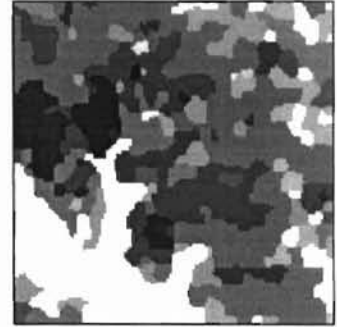
R=90, *V*= 397.3, *MSE*=65.3
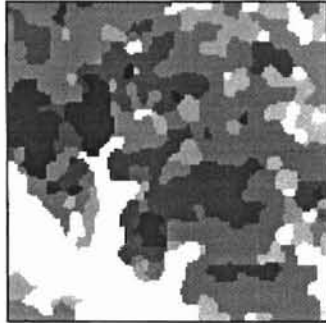
R=80, *V*=441.8, *MSE*=67.1
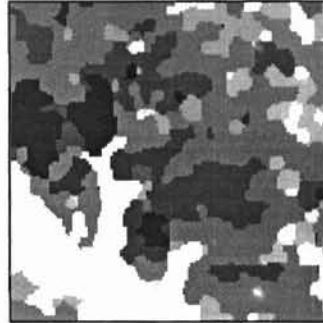
R=70, *V*=445.9, *MSE*=71.3
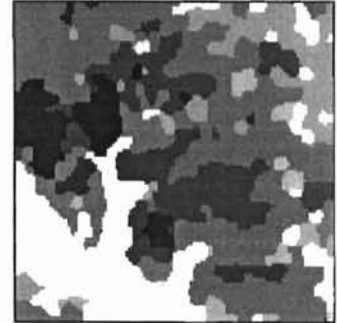
R=60, *V*= 511.8, *MSE*=79.1
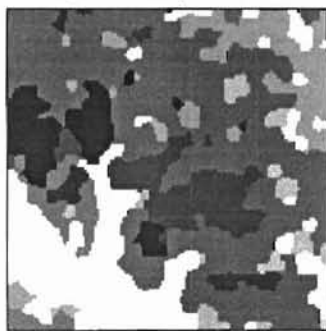
R=50, *V*=587.2, *MSE*=88.1
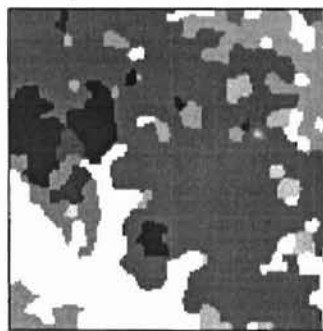
R=40, *V*=605.0, *MSE*=89.1
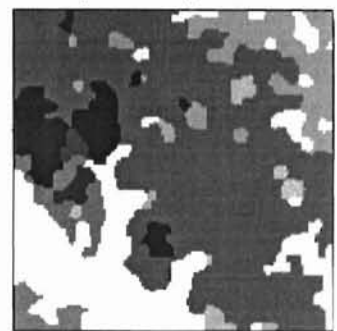
R=30, *V*= 756.1, *MSE*=103.1
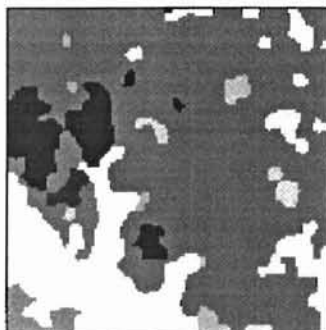
R=20, *V*=1065, *MSE*=134.3
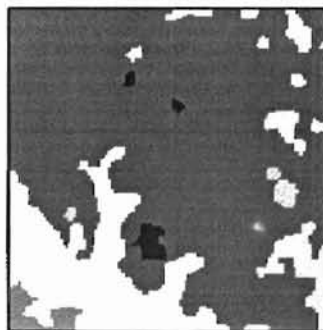
R=10, *V*=1488, *MSE*=166.5

(*R* = the number of regions, *V*= the image variance, *MSE* = the mean squared error)

Fig.5.5(b) SM segmentation results from variational technique on SMr11c10 image

Root Size = 128 : R=553
Original WS Mosaic Image

R=200, V=269.2, MSE=49.1
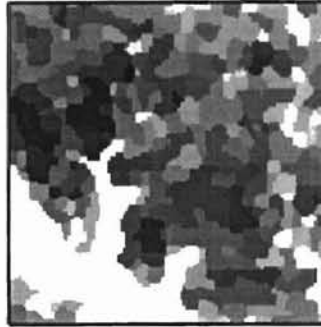
R=100, V=337.2, MSE=56.1
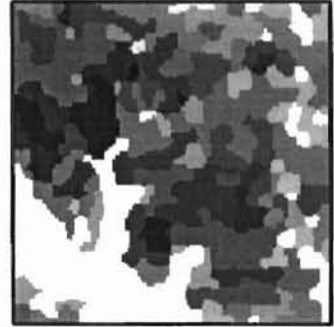
R=90, V= 348.4, MSE=51.6
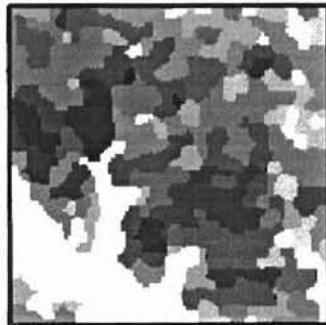
R=80, V=361.1, MSE=54.1
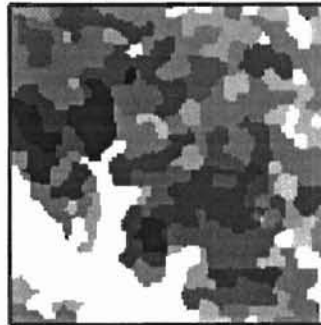
R=70, V=376.4, MSE=61.3
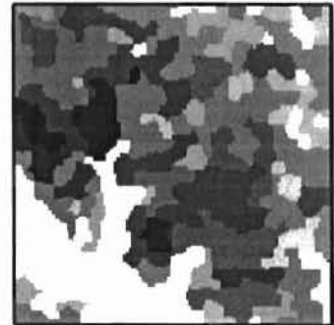
R=60, V= 400.1, MSE=64.6
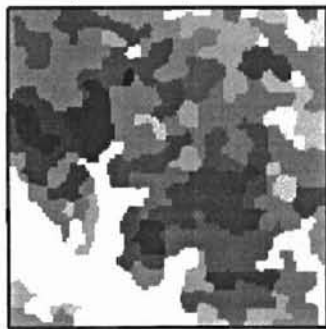
R=50, V=429.7, MSE=67.9
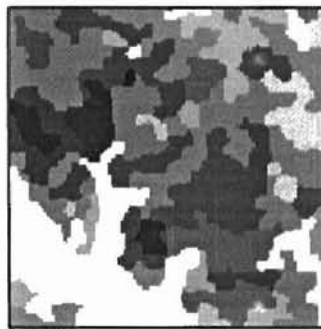
R=40, V=464.9, MSE=72.2
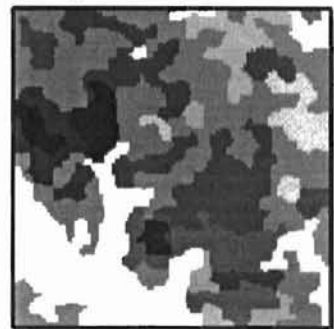
R=30, V= 513.3, MSE=77.6

R=20, V=588.3, MSE=85.2
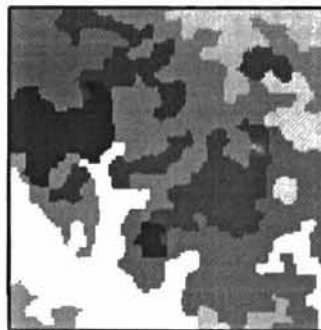
R=10, V=735.9, MSE=104.9
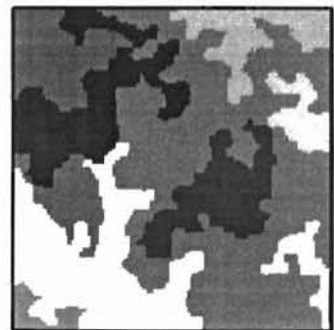
(R = the number of regions, V= the image variance, MSE = the mean squared error)

Fig.5.6 The Edge Maps
(a) The edge map of SMr13c07

Original SM Image
Size = 512
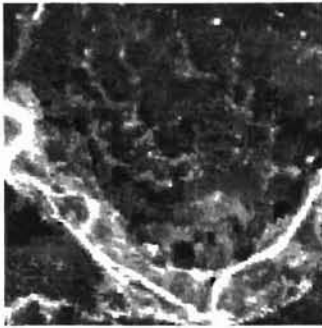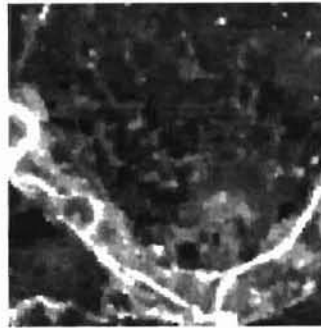
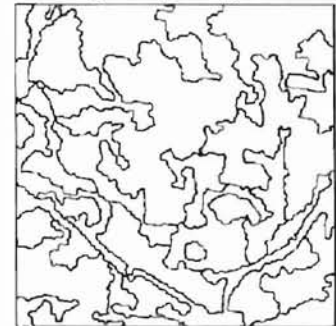SM Image at the root level
Size = 256

The over-segmented WS
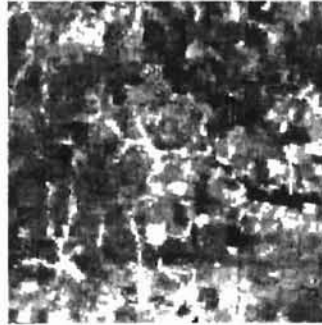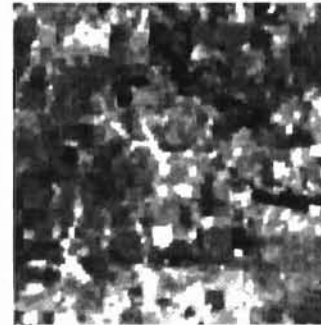Mosaic Image , Size = 256
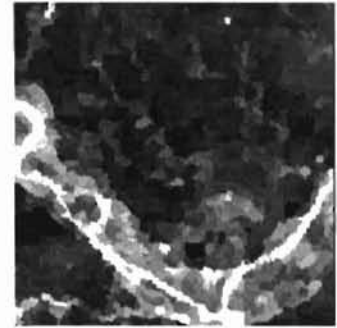
The Merged Image : Region = 30
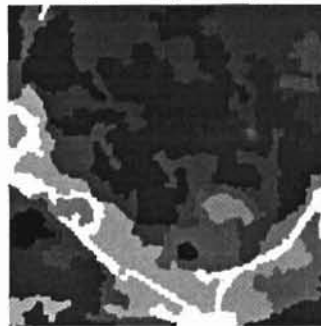
The Edge Map : Region = 30

(b) The edge map of SMr04c04
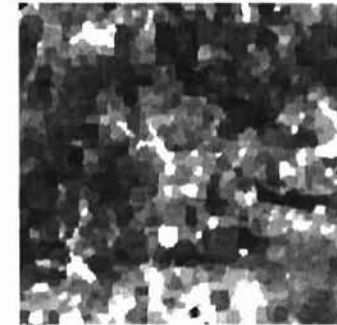
Original SM Image
Size = 512
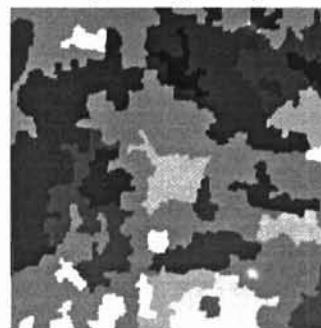
SM Image at the root level
Size = 256

The over-segmented WS
Mosaic Image , Size = 256

The Merged Image : Region = 30

The Edge Map : Region = 30

Fig.5.6 The Edge Maps

(c) The edge map of SMr11c10

Original SM Image
Size = 512

SM Image at the root level
Size = 128

The over-segmented WS
Mosaic Image , Size = 128

The Merged Image : Region = 30
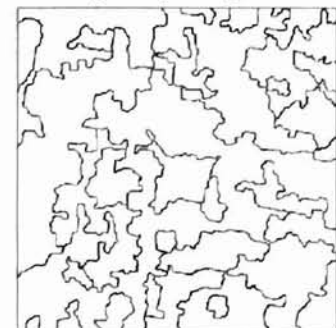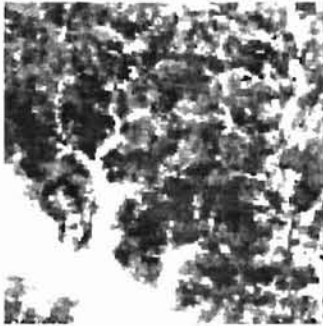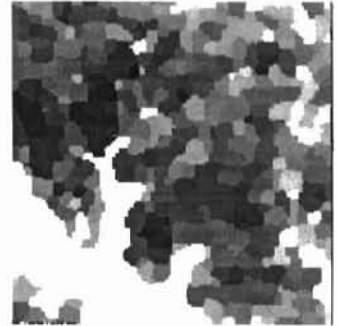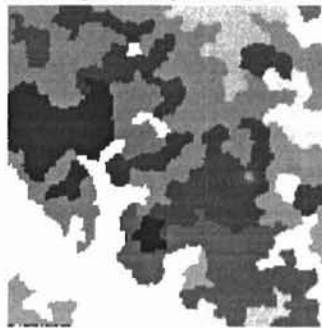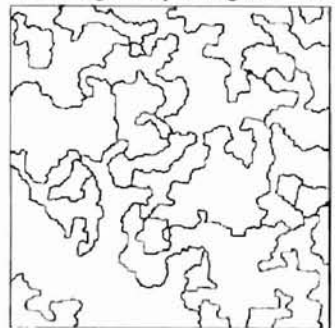
The Edge Map : Region = 30

BIBLIOGRAPHY

Baraldi, A., and Flavio, P., (1996). Single Linkage Region Growing Algorithms Based on the vector degree of Mach. IEEE Transaction of Geo-science and Remote Sensing, Vol.34, No.1 January.

Basara, B.J.,(1997). The Relationship Between Soil Moisture Variation Across Oklahoma and the Daily Oscillation of Moisture in the Planetary Boundary Layer During the Spring of 1997, The University of Oklahoma Master of Science Thesis, http://rossby.metr.ou.edu/~jbasara/research/research.html http://geowww.gcn.ou.edu/WWW/jeff/2291.html

Basara, B.J., and Elliott, R.L.,(1997). IN- SITU MEASUREMENTS OF SOIL MOISTURE FROM THE OKLAHOMA MESONET: MARCH - JUNE 1997, Tenth Symposium on Observations and Instrumentation (Atmospheric Radiation Measurement) Annual Meeting Report, http://geowww.gcn.ou.edu/www/jeff/AMSpreprint.html

Beaulieu, J.M., Goldberg, M., (1989). Hierarchy in Picture Segmentation: A Stepwise Optimization Approach. IEEE Transaction on Pattern Analysis and Machine Intelligence, Vol.11, No.2, February.

Carlson, T.N., Capehart, W.J., and Gillies, R.R.(1995). A New Look at the Simplified Method for Remote Sensing of Daily Evatranspiration.

Carlson[2], T.N., (1995). Soil-Vegetation-Atmosphere Transfer (SVAT) Modeling with Remote Sensing. NASA-EOS Report.

Carlson[3], T.N., and Gilles, R.R., (1995). Thermal Remote Sensing of Surface Soil Water Content with Partial Vegetation Cover for Incorporated into Climate Models. Journal of Applied Meteorology , vol.34, pp. 745-756, April.

Castleman, K. R., (1996). Digital Image Processing, Prentice-Hall Inc., New York.

Dobrin, B.P., Viero, T., and Gabbouj, M. (1994). Fast watershed algorithms: analysis and extensions. Nonlinear Image Processing V, SPIE Vol.2180.

Gonzalez, R.C. and Woods, R.E., (1992). Digital Image Processing, Addison-Wesley Publishing Co., New York.

Goward, S., Nemani, R., Pierce, L., Running, S., (1993). Developing Satellite-derived Estimations of Surface Moisture Status. Journal of Applied Meteorology, Volume32.

Gauch, J. M., and Pizer, S. M. (1993). Multi-resolution Analysis of Ridges and Valley in Gray-Scale Images. IEEE Transaction on Pattern Recognition and Machine Intelligence, Vol.15, No.6, June.

Haralick, R.M. and Shapiro, L.G. (1992). Computer and Robot Vision. Vol.1, Addison-Wesley Publishing co., New York.

Heilman, J.L. and Moore, D.G., (1982). Evaluating Near-Surface Soil Moisture Using Heat Capacity Mapping Mission Data. Remote Sensing of Environment, 12:117-121

Heijmans, H.J. and Toet, A., (1991). Morphological Sampling. CVGIP: Image Understanding, vol.54, pp. 384 – 400.

Jensen, J. R. (1996). Introductory Digital Image Processing : a remote sensing perspective, 2nd edition, Prentice-Hall, Inc., New Jersey .

Li, Wei., Benie, G.B., He, D.C., Wang, S., Ziou, D., and Gwyn, H. Q., (1997). Watershed Based Hierarchical SAR Image Segmentation. International Journal of Remote Sensing (pre approved).

Lillesand, T.M. and Kiefer, R. W., (1994). Remote Sensing and Image Interpretation, John Wiley & Sons, Inc., New York.

Markman, B.L., and Barker, J.L. (1986). Landsat MSS and TM Post-Calibration Dynamic Ranges, Exoatmospheric Reflectances and At-Satellite Temperature. EOSAT Landsat User Notes.

Meyer, F. and Beucher, S. (1990). Morphological Segmentation. Journal of Visual Communication And Image Representation. Vol.1, No.1, September, pp. 21-46.

Meyer, F. and Beucher, S. (1992). The Morphological Approach to Segmentation: The Watershed Transformation. Mathematical Morphology in Image Processing. Marcel Dekker, Inc., New York, pp. 433-481.

Morel, J. M. and Solimini, S., (1994). Variational Methods in Image Segmentation with seven image processing experiments, Brikhauser, Inc., Boston.

Moran, M.S., Jackson, R. D., Raymond L. H. and Gay, L. W. (1989). Mapping Surface Energy Balance Components by Combing Landsat Thematic Mapper and Ground-based Meteorological Data. Remote Sensing and Environment, 30:77-87.

Musick, H.B. and Pelletier, R. E., (1988). Response to Soil Moisture of Spectral Indexes Derived from Bidirectional Reflectance in Thematic Mapper Wavebands. Remote Sensing of Environment, 25:167 – 184.

Morales, A., Acharya, R., and Ko, S.J., (1995). Morphological Pyramids with Alternating Sequential Filters. IEEE Transaction on Image Processing, vol.4, No. 7, July.

Morales, A., and Acharya, R., (1991). An Image Pyramid with morphological Operators. IEEE Transaction on Image Processing, vol.4, No. 7, July.

Price, J.C. (1983). Estimating Surface Temperatures from Satellite Thermal Infrared Data – A Simple Formulation for the Atmospheric Effect. Remote Sensing of Environment, 13:353-361.

Price, J.C. (1980). The potential of Remotely Sensed Thermal Infrared Data to Infer Surface Soil Moisture and Evaporation. Water Resour Res., vol.16, pp. 787-795, Aug.

Shafarenko, L. Petrou, M. (1997). IEEE Transaction of Image. Automated Watershed Segmentation of Randomly Textured Color Images, Vol. 6, No.11, November.

Schott, R., (1989). Image Processing of Thermal Infrared Images. Photogrammetric Engineering and Remote Sensing, Vol. 55, No.9, September, pp. 1311 – 1321.

Shih, S.F. and Jordan, J.D. (1993). Use of Landsat Thermal-IR Data and GIS in Soil Moisture Measurement. Journal of Irrigation and Drainage Engineering, Vol.119, No.5 September/October.

Wegner, S., Harms, T., Oswald, H., and Fleck, E., (1996) The watershed Transformation on Graphs for the Segmentation of CT Image. IEEE Proceedings of ICPR

VITA

Takashi Koshimizu

Candidate for the Degree of

Master of Science

Thesis: WATERSHED SEGMENTATION AND REGION MERGING
WITH APPLICATION TO REMOTE SENSING

Major Field: Electrical Engineering

Biographical:

Personal Data: Born in Ibaragi, Japan, On March 26, 1968, the son of Saburo and
Taeko Koshimizu.

Education: Graduated from Toyodai-Ushiku High School, Ushiku City, Ibaragi,
Japan in March 1986; received Bachelor of Science degree in Electrical
Engineering from Tamagawa University, Tokyo, Japan in March 1990;
received Master of Business Administration from Oklahoma City
University, Oklahoma, in May 1996.
Completed the requirements for the Master of Science degree with a major
in Electrical Engineering at Oklahoma State University in December, 1998.

Experience: Employed as a electrical design engineer by Fujikura Ltd., at Tokyo,
Japan, April 1990 to May 1994. Employed as a graduate research assistant;
Oklahoma State University, Department of Electrical Engineering, 1997 to
present.